A Deterministic Attitude Estimation Using A Single Vector Information and Rate Gyros

A Project Report

submitted by

ABRAHAM P VINOD

(EE09B044)

in partial fulfilment of the requirements

for the award of the degree of

MASTER OF TECHNOLOGY

DEPARTMENT OF Electrical Engineering

INDIAN INSTITUTE OF TECHNOLOGY MADRAS

May 2014

THESIS CERTIFICATE

This is to certify that the thesis titled **A Deterministic Attitude Estimation Using A Single Vector Information and Rate Gyros**, submitted by Abraham P Vinod, to the Indian Institute of Technology, Madras, for the award of the degree of Dual-Degree in Electrical Engineering, is a bona fide record of the research work done by him under our supervision. The contents of this thesis, in full or in parts, have not been submitted to any other Institute or University for the award of any degree or diploma.

Dr. Arun D Mahindrakar
Project Advisor
Associate Professor
Dept. of Electrical Engineering
IIT-Madras 600 036

Dr. Sandipan Bandhopadhyay
Project Co-Advisor
Assistant Professor
Dept. of Engineering Design
IIT-Madras 600 036

Place: Chennai

Date: 30th April 2014

ACKNOWLEDGEMENTS

Acknowledgements are given to people who help you achieve something extraordinary. But when you undergo a transformation in this process, I believe a few kind words will not suffice to express your gratitude towards these positive influences. Overlooking the inadequacy in this approach, I would like to take this opportunity to thank my project guides, Dr. Arun Mahindrakar and Dr. Sandipan Bandhopadyay. Their timely advices and guidance have helped me complete this project in time. While people talk about being at the "right" place at the "right" time, I am lucky to have lived this adage while being under the tutelage of these two mentors.

Any good research requires a good group of researchers. I am thankful to the Dynamics and Control Research Group of IIT Madras. The lively and informative discussions with Vijay, Anup, Chaitanya, Vishaal and Kruthika have helped me shape this project to its current shape. The PhD work of Vijay has served as an experimental testbed for my project and I am deeply grateful for his experience and ideas.

I am also thankful to Dr. Nitin Chandrachoodan and Dr. Sridharan S for their advices. Dr. Nitin, in my second year, gave me an advice which has served as a beacon for my research - *no technical glitch happens without a reason*. Simple as it is, this advice has helped me persevere through the three iterations to finally arrive at this algorithm to estimate the attitude. Dr. Sridharan helped me understand the importance of considering the shortfalls of a processor while developing an algorithm.

I must thank my batchmates and friends who have helped me keep my sanity when my research topic drove me crazy. I would especially like to thank Hersh, Gaurav, Girish and Ameya for their unwavering support for my research pursuits. I thank Nitish, Ankit, Jayant, Soorya, Prakruthi, Meghana, Chitra, Sohini, Jobin, Varun and Vasanth for helping me retain my social skills and stopping me from becoming a complete workaholic. I also thank my batchmates for letting me experience a productive and fun-filled undergraduate life at IIT Madras.

I thank my family for the unwavering support they bestowed upon me while travel-

ling through the ups and downs of this scientific pursuit. Their unrelenting curiosity on the progress of my research work helped me stick to the self-imposed deadlines.

And last but not definitely not the least, I thank God for being beside me at every step in this five year long road.

This project report, therefore, is a testimony of the unconditional support and love showed towards me by my professors, friends and family. I hope I have been able to justify the faith that they have put on me and did justice to the research topic under study.

ABSTRACT

KEYWORDS: Attitude estimate, Inertial Measurement Unit, Special Orthogonal Group.

This project explores a deterministic estimator for the estimation of the attitude of a free rigid body. A deterministic estimator uses a minimal set of information and does not try to minimize a cost function or fit the measurements into a stochastic process. The information set required by the proposed estimator is a single vector information and rate gyro readings. Any vector whose resolution in the body frame can be detected is a potential candidate as a choice for the vector information. The feasibility of the complete attitude estimation from the given input set is demonstrated. For systems in which one of the rotational degrees is constrained, the proposed estimator provides an accurate estimate of the reduced attitude. Special emphasis is made on the computational efficiency of the attitude estimator. Detailed analysis of various sources of error is performed on the algorithm to understand the robustness of the estimator. The algorithm was tested on different testbeds to prove its robustness and accuracy.

TABLE OF CONTENTS

LIST OF TABLES

LIST OF FIGURES

ABBREVIATIONS

DAESR	Deterministic Attitude Estimation using a Single vector and Rate gyros
TRIAD	Tri-axial Attitude Determination

NOTATION

$\boldsymbol{A}$	$\boldsymbol{A} \in \mathbb{R}^{3\times 3}$
$\boldsymbol{a}$	$\boldsymbol{a} \in \mathbb{R}^3$
a	$a \in \mathbb{R}$
$\boldsymbol{\omega}$	Body angular velocity, $\boldsymbol{\omega} \in \mathbb{R}^3$
$\boldsymbol{\Omega}$	Spatial angular velocity, $\boldsymbol{\Omega} \in \mathbb{R}^3$
$\widehat{\boldsymbol{\omega}}$	Skew-symmetric matrix corresponding to the body angular velocity, $\widehat{\boldsymbol{\omega}} \in \mathfrak{so}(3)$
$\widehat{\boldsymbol{\Omega}}$	Skew-symmetric matrix corresponding to the spatial angular velocity, $\widehat{\boldsymbol{\Omega}} \in \mathfrak{so}(3)$
$\boldsymbol{R}_{\boldsymbol{w}\to\boldsymbol{v}}$	$\boldsymbol{R} \in SO(3)$ such that $\boldsymbol{v} = \boldsymbol{R}\boldsymbol{w}$
$\boldsymbol{R}_{\boldsymbol{w}}(\alpha)$	$\boldsymbol{R} \in SO(3)$ such that $\boldsymbol{w} \in S^2$ is the axis of rotation and $\alpha \in S^1$ is the rotation angle
$\boldsymbol{I}_3$	$\boldsymbol{I}_3$ is the 3×3 identity matrix

CHAPTER 1

Introduction

The rotation matrix is an elegant method to capture the transformation between two coordinate frames irrespective of the state of their motion. The matrix helps in determining and explaining several key phenomena seen while studying coordinate frames undergoing relative motion. It also plays a key role in the study of kinematics. Rotation matrices are standard topics in robotic education, e.g, see the established textbooks [1–4]. Rotation matrix's role in the control of attitude problems, e.g, see [5], necessitates the need for methods to infer the attitude of a object using rotation matrices.

1.1 Deterministic and Optimal Attitude Estimators

The problem of estimation of the attitude has been explored quite deeply for past several decades with several novel estimation techniques proposed along the way. These estimators can broadly be classified into two classes - "deterministic" and "optimal" estimators. These terms were popularized by Wertz [6].

The estimators belonging to the deterministic class of estimators use a minimal set of measurements. These estimators obtain the attitude algebraically by solving a set of simultaneous nonlinear equations at every iteration. Deterministic algorithms require exactly three scalar information and in situations when more information is available, suitable constraints are proposed. These estimators have minimal dependence on the measurements taken in the previous iteration. Owing to their algebraic constructs, deterministic algorithms are computationally cheaper but have lesser immunity against measurement noise as compared to optimal estimators [7].

Over the past few decades, technology has taken great strides in packing more computational power in microchips. This has resulted in larger emphasis on optimal class of attitude estimators for their better noise immunity. Optimal estimators try to minimize a cost function, e.g. like Wahba's Problem [8], using a larger set of measurements.

Optimal attitude estimators, because of their stochastic approach, generally provide better estimates of attitude as compared to their deterministic counterparts. Several optimal estimators have been proposed based on Kalman Filters and Complimentary Filters [9–11]. To avoid singularities that arise from parameterizing the rotation matrix as Euler angles, researchers have also explored quarternion based estimation techniques [12]. Shuster developed the QUEST estimator [13] which is one of the most popular optimal estimators and has been widely used in space missions. With the recent advances in image processing, optimal estimation of attitude is also made possible with the help of visual-aids [14].

Deterministic attitude-determination algorithms find application as initial estimate for several optimal algorithms, for e.g. [10], and in applications that have computational constraints hindering it from implementing optimal algorithms. In [7], Shuster analyzes several three-axis deterministic algorithms. They were motivated based on attitude estimation for satellites resulting in the use of arc-length as a scalar measurement apart from a direction information. The TRIAD or the bi-vector method is another deterministic algorithm but utilizes two direction information [7] [15] with the constraint that the direction informations are orthogonal to each other. Direction Cosine Matrix algorithm, which can be classified as a deterministic algorithm, tries to fuse the information provided by the popular nine degree-of-freedom Inertial Measurement Unit (IMU) to estimate the pose of an object [16]. It estimates the attitude by numerically solving a differential equation from two direction informations and the angular rates information.

1.2 Motivation for this dissertation

Our motivation for developing this estimator comes from the realization that in practical scenarios, two direction information may not be available accurately. Moreover, accelerometers can be used to determine the translational velocity of the rigid body in the inertial frame of reference provided the estimated attitude is independent of the accelerometer readings. All the algorithms mentioned in Section 1.1 require the use of accelerometers and magnetometer readings. We pose the following question: *With the information about a constant vector in the inertial frame resolved in the body frame and rate gyro readings, how much information about the attitude can be extracted?* It is

already known that rotation matrix has three degrees of freedom and hence three scalar measurements is needed to uniquely identify the attitude of a body. We demonstrate, in this dissertation, the feasibility of estimating the complete attitude of the rigid body from this constrained input set.

1.3 Contributions of this dissertation

This dissertation proposes a deterministic algorithm to estimate the attitude of a rigid body. The estimator is constructed algebraically leading to a minimal dependence on the history of the motion of the system. The constrained input set defined in Section 1.2 increases the avenues of the practical application of this estimator. Inertial Measurement Unit based estimate of attitude can function as an independent functional block and this is seen from its widespread use in robotics. The single vector information requirement frees the attitude estimation from its dependence on accelerometer. This provides a possibility of accurately estimating translation velocity of the rigid body with respect to inertial frames deterministically.

For systems where certain degrees of rotational freedom is constrained, e.g. mobile inverted pendulum robots [17], the estimator provides an accurate estimation of the reduced attitude of the rigid body which can be numerically integrated to get the complete attitude information [18]. To simulate systems with constrained rotational freedom, the proposed estimator was tested on a Twin-Rotor MIMO System (Figure 5.2). The effectiveness of the proposed estimator in determining the complete attitude was demonstrated through the attitude estimation and dead-reckoning of the position of a spherical robot (Figure 5.4). The heading information of the Mobile Inverted Pendulum, an information unavailable using the conventional attitude estimators, was also obtained to further validate the algorithm (Figure 5.10).

1.4 Organization of this dissertation

We articulate the contributions of this dissertation as follows.

Chapter 2

In this chapter, the mathematical preliminaries helpful in the discussion of the estimator is described. A detailed discussion on the Rodriguez's rotation formula and on the theory of the rotation decomposition used in the estimator.

Chapter 3

Here, we discusses the proposed estimator - DAESR and its related components. The theory developed in this section can be applied to any input set of a single vector information and rate gyros. For simplicity, a framework is defined to elucidate fine points in the development of theory.

Chapter 4

The discussion and analysis of various sources of error in DAESR in this chapter culminates the theoretical work of this dissertation.

Chapter 5

The test results of the algorithm on various experimental testbeds and the analysis of the experimental results is described in this chapter.

Chapter 6

In this final chapter, we summarize the contributions of the thesis and present the concluding remarks.

Appendix A

An alternative estimation procedure for the derivative of a vector lying in S^2 is presented here.

CHAPTER 2

Mathematical Preliminaries

Let $|\cdot|$ denote a norm on $\mathbb{R}^n$. The unit sphere on $\mathbb{R}^n$ is defined as $S^{n-1} = \{\boldsymbol{x} \in \mathbb{R}^n : |\boldsymbol{x}| = 1\}$. $\{\mathbb{F}\}$ denotes an orthogonal coordinate frame. Let $\boldsymbol{I}_3$ denote the 3×3 identity matrix and the orientation of a rigid body be denoted by $\boldsymbol{R}(t) \in SO(3)$ relative to the reference inertial frame, where

$$SO(3) \triangleq \{\boldsymbol{A} \in \mathbb{R}^{3\times 3} : \boldsymbol{A}^\top \boldsymbol{A} = \boldsymbol{I}_3, \det(\boldsymbol{A}) = 1\}$$

and $\dot{\boldsymbol{R}}(t) \in T_{\boldsymbol{R}}SO(3)$, the tangent space to $SO(3)$ at $\boldsymbol{R}$. Since $SO(3)$ is a Lie group, $T_{\boldsymbol{I}}SO(3) \simeq \mathfrak{so}(3)$ acts as Lie algebra of the group, where $\boldsymbol{I}_3$ is the identity element of the group $SO(3)$, $\mathfrak{so}(3)$ is a vector space formed by skew-symmetric matrices. Since $\mathfrak{so}(3)$ is isomorphic to $\mathbb{R}^3$, the wedge operator '$\wedge$', $\boldsymbol{x} \in \mathbb{R}^3 \mapsto \widehat{\boldsymbol{x}} \in \mathfrak{so}(3)$ is defined as

$$\widehat{\boldsymbol{x}} = \begin{bmatrix} 0 & -x_3 & x_2 \\ x_3 & 0 & -x_1 \\ -x_2 & x_1 & 0 \end{bmatrix}$$

Further, let '$\vee$' be the inverse of the wedge operation, that is, $(\hat{\boldsymbol{\omega}})^\vee = \boldsymbol{\omega}$.

Composition of elements in $SO(3)$, the rotation matrices, happens through matrix multiplication. If it is known that $\boldsymbol{R}_{F_2}^{F_1}$ maps vectors in $\{\mathbb{F}_2\}$ to $\{\mathbb{F}_1\}$ and $\boldsymbol{R}_{F_3}^{F_2}$ maps vectors in $\{\mathbb{F}_3\}$ to $\{\mathbb{F}_2\}$, then the rotation matrix that maps vectors from $\{\mathbb{F}_3\}$ to $\{\mathbb{F}_1\}$ is given by $\boldsymbol{R}_{F_3}^{F_1} = \boldsymbol{R}_{F_2}^{F_1}\boldsymbol{R}_{F_3}^{F_2}$ under the group operation.

We represent $\boldsymbol{R}$ as

$$\boldsymbol{R} \triangleq \begin{bmatrix} \boldsymbol{c}_1 & \boldsymbol{c}_2 & \boldsymbol{c}_3 \end{bmatrix} \triangleq \begin{bmatrix} \boldsymbol{r}_1 \\ \boldsymbol{r}_2 \\ \boldsymbol{r}_3 \end{bmatrix} \tag{2.1}$$

where the columns $(\boldsymbol{c}_1, \boldsymbol{c}_2, \boldsymbol{c}_3)$ and the rows $(\boldsymbol{r}_1, \boldsymbol{r}_2, \boldsymbol{r}_3)$ are vectors in S^2. The body angular velocity, $\boldsymbol{\omega} = (\omega_x, \omega_y, \omega_z)$, associated with a rotation is related to the rotation

matrix by the relation $\boldsymbol{\omega} = (\boldsymbol{R}^\top \dot{\boldsymbol{R}})^\vee$. Similarly, the spatial angular velocity matrix, $\boldsymbol{\Omega} = (\Omega_x, \Omega_y, \Omega_z)$, is defined as $\boldsymbol{\Omega} = (\dot{\boldsymbol{R}}\boldsymbol{R}^\top)^\vee$.

2.1 Rodriguez's rotation formula

Proposed in [19], Rodriguez's rotation formula quantifies Euler's angle-axis theorem which states that every rotation matrix $\boldsymbol{R} \in SO(3)$ can be captured in the form of a unit vector acting as the rotation axis and a rotation angle about it [4]. The unit vector acting as the axis is a vector that is invariant to the rotation transformation. This formula is used extensively in applications involving mechanics and image signal processing. The rotation matrix corresponding to a axis-angle pair $(\boldsymbol{\eta}, \theta)$ with $\boldsymbol{\eta} \in S^2, \theta \in S^1$ is given by

$$\boldsymbol{R}_{\boldsymbol{\eta}}(\theta) = \boldsymbol{I}_3 + \widehat{\boldsymbol{\eta}} \sin\theta + \widehat{\boldsymbol{\eta}}^2(1 - \cos\theta). \tag{2.2}$$

Rodriguez's rotation formula can also be used to find the linear transformation $\boldsymbol{R}_{\boldsymbol{w}\to\boldsymbol{v}}$ that maps any two vectors $\boldsymbol{v}, \boldsymbol{w} \in S^2$ by the relation $\boldsymbol{v} = \boldsymbol{R}_{\boldsymbol{w}\to\boldsymbol{v}}\boldsymbol{w}$ as described by Piovan and Bullo [20]. The estimation of $\boldsymbol{R}_{\boldsymbol{w}\to\boldsymbol{v}}$ using (2.2) is based on the axis-angle representation of $\boldsymbol{R}_{\boldsymbol{w}\to\boldsymbol{v}}$ as $\boldsymbol{R}_{\boldsymbol{\eta}}(\theta)$ with,

$$\boldsymbol{\eta} = \frac{\boldsymbol{w} \times \boldsymbol{v}}{|\boldsymbol{w} \times \boldsymbol{v}|} \text{ for } \boldsymbol{v} \neq \pm\boldsymbol{w}, \tag{2.3}$$

$$|\sin\theta| = |\boldsymbol{w} \times \boldsymbol{v}|,$$

$$\cos\theta = \boldsymbol{v}.\boldsymbol{w},$$

$$\theta = \operatorname{atan2}(|\boldsymbol{w} \times \boldsymbol{v}|, \boldsymbol{v}.\boldsymbol{w}). \tag{2.4}$$

Every $\boldsymbol{R} \in SO(3)$ cannot be globally described as $\boldsymbol{R}_{\boldsymbol{\eta}}(\theta)$. This is because a n-dimensional compact manifold cannot be embedded in $\mathbb{R}^n$ without having singularities [4]. This singularity or the condition of indeterminateness occurs when $\boldsymbol{w} = \pm\boldsymbol{v}$. In these scenarios, no unique $\boldsymbol{\eta}$ exists. Apart from this as $\boldsymbol{w}$ approaches $\pm\boldsymbol{v}$, determination of a unit vector $\boldsymbol{\eta}$ becomes increasingly erroneous owing to the division by a very small positive decimal number ($\sin\theta$).

We revisit a modified estimate for $\boldsymbol{R}_{\boldsymbol{w}\to\boldsymbol{v}}$ that avoids the singularity condition at $\theta =$

0 and has a better computational accuracy as presented in [7]. Rodriguez's formula relating unit vectors $\boldsymbol{w}, \boldsymbol{v}$ provided by (2.2), (2.3) and (2.4) can be equivalently written as

$$\begin{aligned} \boldsymbol{R}_{\boldsymbol{w}\to\boldsymbol{v}} &= \boldsymbol{R}_{\boldsymbol{\eta}^*}(\theta) \\ &= \boldsymbol{I}_3 + \widehat{\boldsymbol{\eta}}^* + \frac{(\widehat{\boldsymbol{\eta}}^*)^2}{1+\cos\theta}, \ \forall\, \theta \in S^1/\{\pi\} \end{aligned} \tag{2.5}$$

where

$$\boldsymbol{\eta}^* = \boldsymbol{w} \times \boldsymbol{v}$$
$$\cos\theta = \boldsymbol{w}.\boldsymbol{v}.$$

We note that by fixing the definition of $\boldsymbol{\eta}$ as $\boldsymbol{\eta} = \frac{\boldsymbol{w}\times\boldsymbol{v}}{|\boldsymbol{w}\times\boldsymbol{v}|}$, the axis $\boldsymbol{\eta}$ flips direction depending on the relative orientation of $\boldsymbol{v}$ and $\boldsymbol{w}$. It is for the same reason that estimating θ from (2.4) is allowed since the direction of $\boldsymbol{\eta}$ accounts for the sign of θ.

As seen in Figure 2.1, since the axis is not fixed, $\alpha_1 = \alpha_2$. If the axis is not allowed to flip its direction based on the relative orientation of $\boldsymbol{v}$ and $\boldsymbol{w}$, then $\alpha_1 = -\alpha_2$.

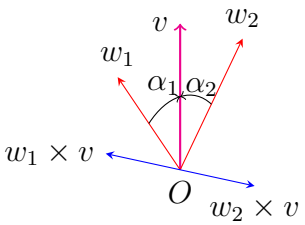

Figure 2.1: Figure demonstrating the discussion on axis-angle pair

2.2 Rotational decomposition used in DAESR

In a recent work on decomposition of rotation matrices into Euler angles [20], Piovan and Bullo provide an decomposition of a rotation matrix linking two vectors. The general rotation matrix linking two vectors $\boldsymbol{v}$ and $\boldsymbol{w}$, according to the work [20], can be

captured by

$$\begin{aligned} \boldsymbol{v} = \boldsymbol{R}\boldsymbol{w} \Rightarrow \boldsymbol{R} &= \exp(\alpha\widehat{\boldsymbol{v}})\exp(\theta\widehat{\boldsymbol{\eta}}) \\ &= \boldsymbol{R}_{\boldsymbol{v}}(\alpha)\boldsymbol{R}_{\boldsymbol{\eta}}(\theta) \end{aligned} \tag{2.6}$$

where $\boldsymbol{e}, \theta$ are provided by the Rodriguez's formula linking $\boldsymbol{w}$ to $\boldsymbol{v}$ and $\alpha \in S^1$.

This interpretation can be geometrically visualized as decomposing any rotation matrix linking two frames as concatenation of two rotation matrices $\boldsymbol{R}_{\boldsymbol{v}}(\alpha)$ and $\boldsymbol{R}_{\boldsymbol{\eta}}(\theta)$. $\boldsymbol{R}_{\boldsymbol{\eta}}(\theta)$ ensures alignment of one of the axes of the body frame to the corresponding axis in the inertial frame. $\boldsymbol{R}_{\boldsymbol{v}}(\alpha)$ aligns the other two axes by rotating about the now aligned axis.

We define a vector correspondence as a set of two vectors which are the resolution of a single free vector resolved in two different coordinate frames. As demonstrated in Section 2.1, $\boldsymbol{R}_{\boldsymbol{\eta}}(\theta)$ can be determined using Rodriguez's formula (2.2) $-$ (2.4). It requires a vector correspondence, that is, the knowledge of the body frame representation of a known vector in inertial frame. To determine $\boldsymbol{R}_{\boldsymbol{v}}(\alpha)$, we need another scalar measurement [7]. As mentioned in the Section 1, TRIAD Algorithm uses another vector correspondence to determine $\boldsymbol{R}_{\boldsymbol{v}}(\alpha)$ with an implicit condition that the constant vectors in the inertial frame are perpendicular to each other [15].

We constraint the input set to a single vector correspondence pair and body angular velocity readings. Although a single vector correspondence implies three scalar measurements, we have an implicit constraint since the rotation matrix preserves the norm of a vector. To obtain the information about the complete attitude, we need to estimate α or $\boldsymbol{R}_{\boldsymbol{v}}(\alpha)$. Since rate gyro readings lie in the velocity space, the rate gyro readings can be used to obtain, at best, an estimate of $\dot{\alpha}$. This holonomic constraint thus provides us an estimate of the reduced attitude in systems which have atleast one constraint in its rotational freedom. This is demonstrated in Section 3.2. For systems where complete attitude estimate is desired, we have to integrate the holonomic constraint. The algorithm is optimized to give the robust estimate of $\dot{\alpha}$ so that the integration is reliable.

We next propose the algorithm for the deterministic estimation of the attitude of the rigid body using a single vector correspondence and rate gyros.

CHAPTER 3

Deterministic attitude estimation using single vector information and rate gyros - DAESR

We use (2.6) to estimate the orientation of an object from the knowledge of a vector $\boldsymbol{v}$, constant in the inertial frame $\boldsymbol{v}_e$, resolved in the body frame along with rate gyro readings. According to the our discussion in Section 2.2, we have to find $\boldsymbol{R}$ such that $\boldsymbol{v}_e = \boldsymbol{R}\boldsymbol{v}$ and $\boldsymbol{R}^\top \dot{\boldsymbol{R}} = \boldsymbol{\omega}$. We have already demonstrated that the given input set falls short in complete attitude estimation since a single vector information provides sufficient information to determine only $\boldsymbol{R}_{\boldsymbol{\eta}}(\theta)$ in (2.6) and rate gyro readings can provide constraints only in the velocity space. In a real world scenario, the constant vector in the inertial frame could be:

1. Earth's gravity (measurable by accelerometer)
2. Earth's magnetic field (measurable by magnetometer)

We postpone the extension of the algorithm using vectors having a time-varying description in inertial frame to Section 3.6.

We assume the following:

- Body coordinate frame of interest $\{\mathbb{B}\}$ is related to the measurement unit coordinate frame $\{\mathbb{G}\}$ by the rotation matrix $\boldsymbol{R}_B^G = \boldsymbol{R}_B$. Note that since the measurement unit is also attached to the body, $\boldsymbol{R}_B$ is a constant matrix.
- Assume an inertial frame $\{\mathbb{I}\}$ which has one of its axes along the direction of $\boldsymbol{v}_e$ and rotated about $\boldsymbol{v}_e$ so that $\{\mathbb{I}\}$ coincides with $\{\mathbb{G}\}$ at the start of the experiment. Inertial coordinate frame of interest $\{\mathbb{I}_0\}$ for the estimator is related to the frame $\{\mathbb{I}\}$ by rotation matrix $\boldsymbol{R}_I^{I_0} = \boldsymbol{R}_I$. Note that since $\{\mathbb{I}\}$ and $\{\mathbb{I}_0\}$ are inertial frames, $\boldsymbol{R}_I$ is a constant matrix.
- Assume an intermediary non-inertial coordinate frame $\{\mathbb{I}_1\}$, which is a coordinate frame obtained by rotating $\{\mathbb{I}\}$ by $\alpha \in S^1$ about $\boldsymbol{v}_e$, $\boldsymbol{R}_{I_1}^I = \boldsymbol{R}_{\boldsymbol{v}_e}(\alpha)$. At the start of the experiment, $\alpha = 0$ causing $\{\mathbb{I}_1\}$ to coincide with $\{\mathbb{I}\}$ and $\{\mathbb{G}\}$.

The rotational displacement between a non-inertial coordinate frame $\{\mathbb{B}\}$ and an inertial coordinate frame $\{\mathbb{I}_0\}$ is given by

$$\begin{aligned}\boldsymbol{R} = \boldsymbol{R}_B^{I_0} &= \boldsymbol{R}_I^{I_0}\boldsymbol{R}_{I_1}^{I}\boldsymbol{R}_G^{I_1}\boldsymbol{R}_B^G \\ &= \boldsymbol{R}_I\boldsymbol{R}_{\boldsymbol{v}_e}(\alpha)\boldsymbol{R}_{\boldsymbol{v}\to\boldsymbol{v}_e}\boldsymbol{R}_B. \end{aligned} \tag{3.1}$$

We now construct a framework which will help in simplifying and motivating further discussions.

3.1 Formulation of attitude estimation problem

Consider the problem of estimating the attitude of a rigid body using accelerometer reading ($\boldsymbol{a}$) and rate gyro sensors. Under low body acceleration conditions, the accelerometer picks up the approximate resolution of earth's gravity. Since $\boldsymbol{R}_I, \boldsymbol{R}_B$ are known *a priori* and do not appear in the measurements, we can consider without loss of generality $\boldsymbol{R}_I = \boldsymbol{R}_B = \boldsymbol{I}_3$. We define a framework as follows

$$\boldsymbol{v} \to \boldsymbol{a},\ \boldsymbol{v}_e \to -\boldsymbol{e}_3$$

where $\{\mathbb{I}\} = \{\mathbb{I}_0\} = \{\boldsymbol{e}_1, \boldsymbol{e}_2, \boldsymbol{e}_3\}$, $\{\mathbb{I}_1\} = \{\boldsymbol{e}_1^*, \boldsymbol{e}_2^*, \boldsymbol{e}_3^*\}$ and $\{\mathbb{G}\} = \{\mathbb{B}\} = \{\boldsymbol{e}_1', \boldsymbol{e}_2', \boldsymbol{e}_3'\}$, $\boldsymbol{e}_i$ are the standard basis vectors in $\mathbb{R}^3$.

We can, thus, define the attitude of $\{\mathbb{B}\}$ as seen from $\{\mathbb{I}_0\}$ as $\boldsymbol{R}_{\text{est}}$ given by

$$\begin{aligned}\boldsymbol{R}_{\text{est}} &= \boldsymbol{R}_I^{I_0}\boldsymbol{R}_{I_1}^{I}\boldsymbol{R}_G^{I_1}\boldsymbol{R}_B^G \\ &= \boldsymbol{R}_{I_1}^{I}\boldsymbol{R}_G^{I_1} \\ &= \exp\left(\alpha^-\widehat{\boldsymbol{v}}_e\right)\exp\left(\theta\widehat{\boldsymbol{\eta}}\right) \\ &= \exp\left(\alpha^-(-\widehat{\boldsymbol{e}}_3)\right)\exp\left(\theta\widehat{\boldsymbol{\eta}}\right) \\ &= \exp\left(\alpha\widehat{\boldsymbol{e}}_3\right)\exp\left(\theta\widehat{\boldsymbol{\eta}}\right) \\ &= \boldsymbol{R}_{\boldsymbol{z}}(\alpha)\boldsymbol{R}_{\boldsymbol{v}\to\boldsymbol{v}_e} \end{aligned} \tag{3.2}$$

where $\alpha = -\alpha^- \in S^1$.

Figure 3.1 captures the transitions undergone during the attitude estimation. The

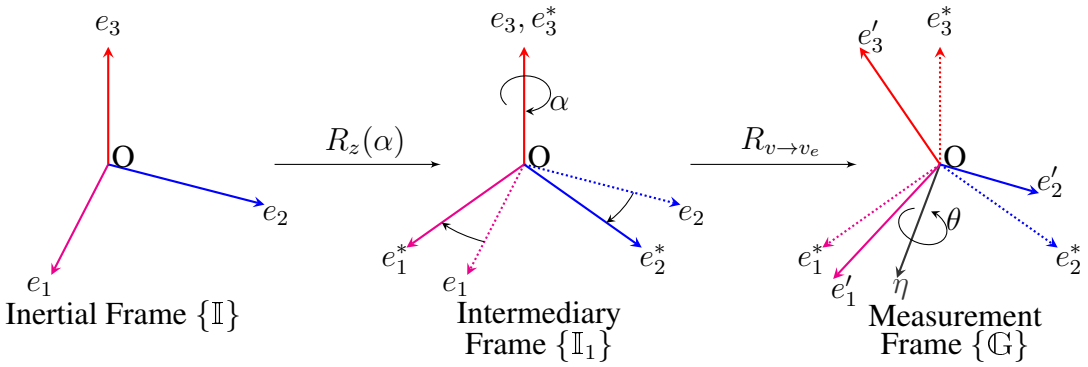

Figure 3.1: Frames for a typical attitude estimation with $\boldsymbol{R}_I = \boldsymbol{R}_B = \boldsymbol{I}_3$

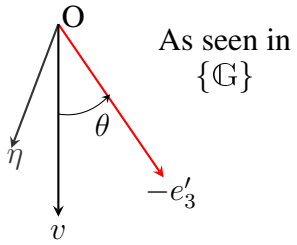

Figure 3.2: Determining η

order of the cross-product is defined by the fact that we have to map the vector $\boldsymbol{e}_3^*$ to $\boldsymbol{e}_3'$ and since $-\boldsymbol{e}_3^*$ in $\{\mathbb{G}\}$ is $\boldsymbol{v}$ and $-\boldsymbol{e}_3'$ in $\{\mathbb{G}\}$ is $\boldsymbol{v}_e$, $\boldsymbol{\eta}$ is determined by $\frac{\boldsymbol{v}\times\boldsymbol{v}_e}{|\boldsymbol{v}\times\boldsymbol{v}_e|}$. Figure 3.2 describes the determination of $\boldsymbol{\eta}$.

3.2 Determination of $\boldsymbol{R}_{\boldsymbol{v}\to\boldsymbol{v}_e}$

The modified estimate for Rodriguez's rotation formula proposed in Section 2.1 is used to estimate $\boldsymbol{R}_{\boldsymbol{v}\to\boldsymbol{v}_e}$. Although, this modified estimate improves the computational accuracy and provides a guarantee against singularity conditions, the estimation given by (2.5) cannot be applied for all $\boldsymbol{v} \in S^2$. This is because the equation involves a division with the term $1 + \cos\theta$. Dividing by a number by a decimal number $f \in [0, 0.5]$ introduces significant amount of error. Hence, the use of (2.5) to determine $\boldsymbol{R}_{\boldsymbol{v}\to\boldsymbol{v}_e}$ is constrained to the condition $\theta \in [-\theta_t, \theta_t]$ where $\theta_t \in S^1$ such that $(1 + \cos\theta) \notin [0, 0.5]$. We motivate the value of θ_t at the end of this section.

Define $S_L = \{\theta \in S^1 : \theta \in [-\theta_t, \theta_t]\}$ and $S_U = S^1 \setminus S_L$. For $\theta \in S_U$, we can utilize Euler angle convention (ψ, δ, γ) to obtain $\boldsymbol{R}_{\boldsymbol{v}\to\boldsymbol{v}_e}$. We now motivate our choice of Euler angle convention (ψ, δ, γ).

1. *Determining all Euler angles is not feasible*: As discussed earlier in Section 2.1, a

Algorithm 1 Algorithm for obtaining $\boldsymbol{R}_{\boldsymbol{v}\to\boldsymbol{v}_e}$

procedure RVRODRIGUEZ($\boldsymbol{v}, \boldsymbol{v}_e$)
  $\cos\theta \leftarrow \boldsymbol{v}.\boldsymbol{v}_e$ ▷ Determining $\cos\theta$ - Eq. (2.4)
  $\boldsymbol{\eta} \leftarrow \boldsymbol{v} \times \boldsymbol{v}_e$ ▷ Determining $\boldsymbol{\eta}$ - Eq. (2.3)
  $\boldsymbol{K} \leftarrow (\boldsymbol{\eta})^{\wedge}$ ▷ Wedge operator acting on $\boldsymbol{\eta}$
  $\boldsymbol{R}_r \leftarrow \boldsymbol{I}_3 + \boldsymbol{K} + \frac{\boldsymbol{K}^2}{1+\cos\theta}$ ▷ From Eq. (2.5)
  return $\boldsymbol{R}_r$
end procedure

single vector correspondence can help in unique determination of δ and γ alone. Hence, ψ cannot be determined. To determine ψ, a possible solution is to ensure that the choice of the Euler angle convention is such that its rightmost axis is aligned along $\boldsymbol{v}_e$. This allows us to combine the rotations about $\boldsymbol{v}_e$, $\boldsymbol{R}_{\boldsymbol{v}_e}(\alpha)$ and $\boldsymbol{R}_{\boldsymbol{v}_e}(\psi)$, as a single rotation.

2. *Singularity condition of the Euler angle convention*: Euler angle convention, by definition, has two singularity points. The choice of the convention should allow S_U to be a singularity-free set.

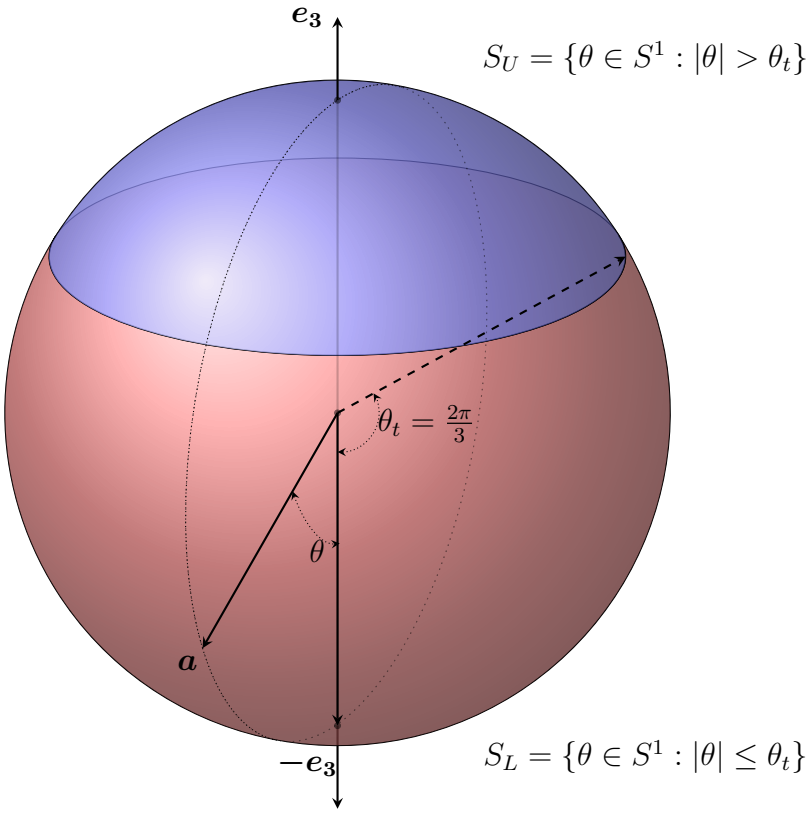

Figure 3.3: Figure explaining the discussion on the θ_t, S_L and S_U

Let $\boldsymbol{R}_{\text{part}}$ be the rotation matrix formed using the knowledge of Euler angles δ and γ. Although $\boldsymbol{R}_{\text{part}}$ is sufficient to align $\boldsymbol{v}_e$ to $\boldsymbol{v}$, the estimate for $\boldsymbol{R}_{\boldsymbol{v}\to\boldsymbol{v}_e}$ needs to match with the theoretical estimate arrived at from the application of Rodriguez's formula. Since

the constraint of vector correspondence is satisfied, the only constraint that is left for this estimate of $\boldsymbol{R}_{\boldsymbol{v}\to\boldsymbol{v}_e}$ to satisfy is the alignment of the axis. We know, from (2.3), that the axis of $\boldsymbol{R}_{\boldsymbol{v}\to\boldsymbol{v}_e}$ is constrained in a plane perpendicular to $\boldsymbol{v}_e$. Hence, a rotational correction of ψ about $\boldsymbol{v}_e$ would be sufficient to align the axes of rotation $-$ the theoretical estimate of the axis (2.3) and the effective axis of rotation $\boldsymbol{R}_{\text{part}}$. Since the theoretical estimate for the axis has a singularity associated with it (when $\boldsymbol{v} = -\boldsymbol{v}_e$), ψ cannot be determined analytically in S_U.

For the framework described in Section 3.1, we choose ZYX notation for the Euler Angle convention. Apart from satisfying the first condition, since the ZYX Euler angle notation has a singularity when $\delta = \pm\frac{\pi}{2}$, we have a singularity free set as S_U. The lesser popular ZXY Euler angle convention is also a viable option, but Euler angle conventions ZYZ and ZXZ cannot be used since they have a singularity at $\theta = \pi$ which lies in S_U.

Choice of ZYX Euler angle notation allows for the redefinition of $\boldsymbol{R}_{\boldsymbol{v}\to\boldsymbol{v}_e}$ as $\boldsymbol{R}_{\boldsymbol{v}\to\boldsymbol{v}_e} = \boldsymbol{R}_{\boldsymbol{z}}(\psi)\boldsymbol{R}_{\boldsymbol{y}}(\delta)\boldsymbol{R}_{\boldsymbol{x}}(\gamma)$. If $\boldsymbol{v}$ comes arbitrarily close to $\boldsymbol{e}_1'$ ($\boldsymbol{x}$-axis of $\mathbb{G}$), then γ becomes indeterminate. This is the manifestation of the singularity at $\delta = \pm\frac{\pi}{2}$ in the framework defined by Section 3.1. The choice of θ_t ensures an arbitrary small open set containing $\delta = \pm\frac{\pi}{2}$ is not a subset of S_U.

Using θ_t to partition S^1 into S_L and S_U, we can redefine $\boldsymbol{R}_{\text{est}}$ from (3.1) as follows

$$\boldsymbol{R}_{\text{est}} = \begin{cases} \boldsymbol{R}_{\boldsymbol{z}}(\alpha)\boldsymbol{R}_{\boldsymbol{v}\to\boldsymbol{v}_e} & \theta \in S_L \\ \boldsymbol{R}_{\boldsymbol{z}}(\alpha)\boldsymbol{R}_{\boldsymbol{z}}(\psi)\boldsymbol{R}_{\boldsymbol{y}}(\delta)\boldsymbol{R}_{\boldsymbol{x}}(\gamma) & \theta \in S_U. \end{cases} \tag{3.3}$$

For $\theta \in S_U$, $\boldsymbol{R}_{\boldsymbol{z}}(\alpha)\boldsymbol{R}_{\boldsymbol{z}}(\psi)$ can be combined as $\boldsymbol{R}_{\boldsymbol{z}}(\alpha+\psi)$ as discussed earlier. The rotation about the z-axis of $\{\mathbb{I}_1\}$, $\boldsymbol{e}_3$, to align $\{\mathbb{I}_1\}$ to $\{\mathbb{I}\}$ is still unknown. The rate of rotation about $\boldsymbol{e}_3$ can be obtained from the rate gyro readings as discussed in Section 2.2. $\boldsymbol{R}_{\boldsymbol{z}}(\alpha+\psi)$ is, then, obtained from integrating the rate of rotation about $\boldsymbol{e}_3$. Estimation of the rate of rotation about $\boldsymbol{e}_3$ is deferred for Section 3.3.

Since an attitude estimator needs to be smooth, we need to ensure continuity in the attitude estimation at the boundary of S_L and S_U, $\theta = \theta_t$. We ensure this by modifying (3.3) to include an integration constant $\boldsymbol{R}_C$ which is a rotation about $\boldsymbol{e}_3$, by definition. Defining $\boldsymbol{R}_L$ and $\boldsymbol{R}_U$ as the attitude estimates for the respective sets S_L and S_U,

we have

$$\boldsymbol{R}_{\text{est}} = \begin{cases} \boldsymbol{R}_L & \theta \in S_L \\ \boldsymbol{R}_U & \theta \in S_U \end{cases}$$
$$= \begin{cases} \boldsymbol{R}_{\boldsymbol{z}}(\alpha)\boldsymbol{R}_C\boldsymbol{R}_{\boldsymbol{v}\to\boldsymbol{v}_e} & \theta \in S_L \\ \boldsymbol{R}_{\boldsymbol{z}}(\alpha+\psi)\boldsymbol{R}_C\boldsymbol{R}_{\boldsymbol{y}}(\delta)\boldsymbol{R}_{\boldsymbol{x}}(\gamma) & \theta \in S_U. \end{cases}$$

The estimation starts with $\boldsymbol{R}_C = \boldsymbol{I}_3$ and $\alpha = \psi = 0$. When v crosses the boundary, we estimate the orientation $\boldsymbol{R}_{\text{est}}$ using the previous set's estimation formula and set $\alpha = 0$. The integration constant do not change value as long as θ does not cross the common boundary S_L and S_U, $\theta = \theta_t$.

$$\boldsymbol{R}_C = \begin{cases} \boldsymbol{R}_L\boldsymbol{R}_{\boldsymbol{x}}^\top(\gamma)\boldsymbol{R}_{\boldsymbol{y}}^\top(\delta) & S_L \to S_U \\ \boldsymbol{R}_U\boldsymbol{R}_{\boldsymbol{v}\to\boldsymbol{v}_e}^\top & S_U \to S_L. \end{cases} \tag{3.4}$$

The assumption used is that the estimates $\boldsymbol{R}_L$ and $\boldsymbol{R}_U$ are both reliable in the neighbourhood of the boundary $\theta = \theta_t$. This requires a good margin from the singularity of the Euler angle decomposition of $\boldsymbol{R}_{\boldsymbol{v}\to\boldsymbol{v}_e}$. To achieve a good margin from the singularity condition and to have a numerically stable estimate of $\frac{1}{1+\cos\theta}$, we choose $\theta_t = \frac{2\pi}{3}$. For $\theta_t = \frac{2\pi}{3}$, $\frac{1}{1+\cos\theta} \in [0.5, 2]$. Sampling rate of the sensors must ensure that the margin provided by the choice of θ_t is not breached. Figure 3.3 explains the discussion on the θ_t, S_L and S_U.

To complete the integration, we redefine the estimated attitude given by (3.2) as,

$$\boldsymbol{R}_{\text{est}} = \boldsymbol{R}_A\boldsymbol{R}_V \tag{3.5}$$

where,

$$\boldsymbol{R}_A = \begin{cases} \boldsymbol{R}_{\boldsymbol{z}}(\alpha)\boldsymbol{R}_C & \theta \in S_L \\ \boldsymbol{R}_{\boldsymbol{z}}(\alpha+\psi)\boldsymbol{R}_C & \theta \in S_U \end{cases}$$
$$\boldsymbol{R}_V = \begin{cases} \boldsymbol{R}_{\boldsymbol{v}\to\boldsymbol{v}_e} & \theta \in S_L \\ \boldsymbol{R}_{\boldsymbol{y}}(\delta)R_{\boldsymbol{x}}(\gamma) & \theta \in S_U. \end{cases}$$

By definition, the axis of $\boldsymbol{R}_A$ is always parallel to $\boldsymbol{v}_e$ and $\boldsymbol{v}_e = \boldsymbol{R}_V \boldsymbol{v}$.

For $\theta \in S_U$, $\boldsymbol{R}_V = \boldsymbol{R_y}(\delta) R_{\boldsymbol{x}}(\gamma)$,

$$\boldsymbol{R}_V = \begin{bmatrix} \cos\delta & \sin\gamma\sin\delta & \cos\gamma\sin\delta \\ 0 & \cos\gamma & -\sin\gamma \\ -\sin\delta & \cos\delta\sin\gamma & \cos\gamma\cos\delta \end{bmatrix}$$

and

$$\boldsymbol{R}_{\boldsymbol{v}\to\boldsymbol{v}_e} = \boldsymbol{R_z}(\psi)\boldsymbol{R}_V.$$

As discussed earlier, we have two constraints:

1. $-\boldsymbol{e}_3 = \boldsymbol{R_z}(\psi)\boldsymbol{R}_V\boldsymbol{a}$.
2. axis of $\boldsymbol{R}_{\boldsymbol{v}\to\boldsymbol{v}_e}$ is given by (2.3).

Solving for the constraint $-\boldsymbol{e}_3 = \boldsymbol{R}_V\boldsymbol{a}$ provides a solution for $\boldsymbol{R}_V$. For $a = (a_x, a_y, a_z)$,

$$\begin{aligned} \sin\delta &= \pm\, a_x \\ \cos\delta &= \pm\, \sqrt{a_y^2 + a_z^2} \\ \cos\gamma &= \mp\, \frac{a_z}{\sqrt{a_y^2 + a_z^2}} \\ \sin\gamma &= \mp\, \frac{a_y}{\sqrt{a_y^2 + a_z^2}}. \end{aligned}$$

On substitution, $\boldsymbol{R}_V$ becomes,

$$\begin{aligned} \boldsymbol{R}_V &= \begin{bmatrix} \pm\sqrt{a_y^2+a_z^2} & \mp\frac{a_x a_y}{\sqrt{a_y^2+a_z^2}} & \mp\frac{a_x a_z}{\sqrt{a_y^2+a_z^2}} \\ 0 & \mp\frac{a_z}{\sqrt{a_y^2+a_z^2}} & \pm\frac{a_y}{\sqrt{a_y^2+a_z^2}} \\ -a_x & -a_y & -a_z \end{bmatrix} \\ &= \boldsymbol{R}_Z(\tau) \begin{bmatrix} \sqrt{a_y^2+a_z^2} & -\frac{a_x a_y}{\sqrt{a_y^2+a_z^2}} & -\frac{a_x a_z}{\sqrt{a_y^2+a_z^2}} \\ 0 & -\frac{a_z}{\sqrt{a_y^2+a_z^2}} & \frac{a_y}{\sqrt{a_y^2+a_z^2}} \\ -a_x & -a_y & -a_z \end{bmatrix} \end{aligned}$$

where $\tau \in \{0, \pi\}$.

Since $\boldsymbol{R}_C$ is also a rotation about z-axis, $\boldsymbol{R_z}(\tau)$ gets absorbed into the integration constant. Thus, for $\theta \in S_U$,

$$\begin{aligned}\boldsymbol{R}_V &= \boldsymbol{R_y}(\delta)R_{\boldsymbol{x}}(\gamma) \\ &= \begin{bmatrix} \sqrt{a_y^2+a_z^2} & -\frac{a_x a_y}{\sqrt{a_y^2+a_z^2}} & -\frac{a_x a_z}{\sqrt{a_y^2+a_z^2}} \\ 0 & -\frac{a_z}{\sqrt{a_y^2+a_z^2}} & \frac{a_y}{\sqrt{a_y^2+a_z^2}} \\ -a_x & -a_y & -a_z \end{bmatrix}. \end{aligned} \tag{3.6}$$

Furthermore, ψ can be estimated by imposing the constraint on the axis of $\boldsymbol{R}_{\boldsymbol{v}\to\boldsymbol{v}_e}$. This gives the result, for $\tau = 0$,

$$\begin{aligned}\sin\psi &= \frac{-a_x a_y}{(1-a_z)\sqrt{a_y^2+a_z^2}} \\ \cos\psi &= \frac{1-a_z-a_x^2}{(1-a_z)\sqrt{a_y^2+a_z^2}}.\end{aligned}$$

As expected, this estimate of ψ is not numerically stable since S_U contains $a_z = 1$. This is the motivation for absorbing $\boldsymbol{R_z}(\psi)$ into $\boldsymbol{R}_A$.

Since $\boldsymbol{R_z}(\psi)$ has been assigned as a part of $\boldsymbol{R}_A$, $\boldsymbol{R}_V$ and $\boldsymbol{R}_A$ are piecewise continuous maps with discontinuity at the boundary $\theta = \theta_t$. Continuity of $\boldsymbol{R}_{\text{est}}$ is ensured through the introduction of $\boldsymbol{R}_C$.

While Shuster in his discussion of deterministic algorithms [7] uses only the modified Rodriguez's formula discussed in Section 2.1, the approach of splitting the sphere into separate sets, S_L and S_U will ensure higher numerical stability. This has been verified in the experiments described in Chapter 5.

3.3 Determination of $\boldsymbol{R}_A$

We note that the construction of (3.5) is solely motivated by practical constraints. This construction helps in decomposing (3.1) into components that can be obtained numerically. $\boldsymbol{R}_{\boldsymbol{v}\to\boldsymbol{v}_e}$ is geometrically understood as the rotation matrix that aligns $\boldsymbol{v}$ to $\boldsymbol{v}_e$. Since $\boldsymbol{v}_e$ is a constant vector and $\boldsymbol{v}$ is the resolution of the vector in the body frame, $\boldsymbol{R}_{\boldsymbol{v}\to\boldsymbol{v}_e}$ is a physical property of the system and hence is continuous and differentiable.

Continuing on this argument, we can see that $\boldsymbol{R_z}(\alpha)$ is also differentiable.

Consider the spatial angular velocity $\widehat{\boldsymbol{\Omega}}$ of the frame $\{\mathbb{B}\}$ as seen from $\{\mathbb{I}_0\}$ based on the definition given by (3.2),

$$\begin{aligned}\widehat{\boldsymbol{\Omega}} &= \dot{\boldsymbol{R}}_{\text{est}}\boldsymbol{R}_{\text{est}}^{\top} \\ &= (\dot{\boldsymbol{R}}_a\boldsymbol{R}_{\boldsymbol{v}\to\boldsymbol{v}_e} + \boldsymbol{R_z}(\alpha)\dot{\boldsymbol{R}}_v)\boldsymbol{R}_{\boldsymbol{v}\to\boldsymbol{v}_e}^{\top}\boldsymbol{R_z}(\alpha)^{\top} \\ &= \widehat{\boldsymbol{\Omega}}_a + \boldsymbol{R_z}(\alpha)\widehat{\Omega}_v\boldsymbol{R_z}(\alpha)^{\top}. \end{aligned} \tag{3.7}$$

For $\theta \in S_L$, we transform (3.7) to the corresponding vector space through similarity transform and the application of $\vee$ operator. The body angular velocity vector $\boldsymbol{\omega}$ is obtained from rate gyro readings.

$$\boldsymbol{\Omega} = \boldsymbol{\Omega}_a + \boldsymbol{R_z}(\alpha)\boldsymbol{\Omega}_v.$$

But $\boldsymbol{\Omega} = \boldsymbol{R}_{\text{est}}\boldsymbol{\omega} = \boldsymbol{R_z}(\alpha)\boldsymbol{R}_{\boldsymbol{v}\to\boldsymbol{v}_e}\boldsymbol{\omega}$ and hence,

$$\boldsymbol{R_z}(\alpha)\boldsymbol{R}_{\boldsymbol{v}\to\boldsymbol{v}_e}\boldsymbol{\omega} = \boldsymbol{\Omega}_a + \boldsymbol{R_z}(\alpha)\boldsymbol{\Omega}_v. \tag{3.8}$$

Under the framework described in Section 3.1, $\boldsymbol{R_z}(\alpha)$ is a rotation about $\boldsymbol{e}_3$ by $\alpha \in S^1$.

$$\boldsymbol{\Omega}_a = \boldsymbol{\omega}_a = \begin{bmatrix} 0 \\ 0 \\ \dot{\alpha} \end{bmatrix}$$

$$\Rightarrow \boldsymbol{R_z}(\alpha)^{\top}\boldsymbol{\Omega}_a = \boldsymbol{R_z}(\alpha)\boldsymbol{\Omega}_a = \boldsymbol{\Omega}_a.$$

Thus, (3.8) simplifies to

$$\boldsymbol{R}_{\boldsymbol{v}\to\boldsymbol{v}_e}\boldsymbol{\omega} = \begin{bmatrix} 0 \\ 0 \\ \dot{\alpha} \end{bmatrix} + \boldsymbol{\Omega}_v. \tag{3.9}$$

For $\theta \in S_U$, if $\boldsymbol{R}_C$ is represented as $\boldsymbol{R_z}(c)$ for some $c \in S^1$, we know that

$$\boldsymbol{R}_{\text{est}} = \boldsymbol{R}_Z(\alpha + \psi + c)R_{\boldsymbol{y}}(\delta)R_{\boldsymbol{x}}(\gamma).$$

Hence, (3.7) is modified to replace $\boldsymbol{\Omega}_a$ with $\boldsymbol{\Omega}_z$ and $\boldsymbol{\Omega}_v$ with $\boldsymbol{\Omega}_{yx}$,

$$\widehat{\boldsymbol{\Omega}} = \widehat{\boldsymbol{\Omega}}_z + \boldsymbol{R_z}(\alpha+\psi+c)\widehat{\boldsymbol{\Omega}}_{yx}\boldsymbol{R_z}^\top(\alpha+\psi+c). \tag{3.10}$$

Repeating the analysis done for $\theta \in S_L$, we get from (3.10),

$$\boldsymbol{R_y}(\delta)\boldsymbol{R_x}(\gamma)\boldsymbol{\omega} = \begin{bmatrix} 0 \\ 0 \\ \dot{\alpha} \end{bmatrix} + \begin{bmatrix} 0 \\ 0 \\ \dot{\psi} \end{bmatrix} + \boldsymbol{\Omega}_{yx}. \tag{3.11}$$

The independence of $\boldsymbol{R_z}(\alpha)$ while transitioning from (3.8) to (3.9) and (3.10) to (3.11) is in agreement with our analysis in Section 2.2. We have mathematically demonstrated that a single vector information and rate gyro readings will not be sufficient to determine the complete attitude without integration.

Equations (3.9) and (3.11) can be combined with (3.5) to obtain a simplified expression

$$\boldsymbol{R}_V\boldsymbol{\omega} = \boldsymbol{\Omega}_A + \boldsymbol{\Omega}_V \tag{3.12}$$

where

$$\boldsymbol{\Omega}_A = \begin{cases} \dot{\alpha}\boldsymbol{e}_3 & \theta \in S_L \\ (\dot{\alpha}+\dot{\psi})\boldsymbol{e}_3 & \theta \in S_U. \end{cases}$$

Rewriting (3.12) component-wise,

$$\boldsymbol{e}_3^\top\boldsymbol{\Omega}_A = \boldsymbol{e}_3^\top(\boldsymbol{R}_V\boldsymbol{\omega} - \boldsymbol{\Omega}_V) \tag{3.13}$$

$$\boldsymbol{e}_1^\top\boldsymbol{\Omega}_V = \boldsymbol{e}_1^\top\boldsymbol{R}_V\boldsymbol{\omega} \tag{3.14}$$

$$\boldsymbol{e}_2^\top\boldsymbol{\Omega}_V = \boldsymbol{e}_2^\top\boldsymbol{R}_V\boldsymbol{\omega}. \tag{3.15}$$

Equation (3.13) gives the estimate of $\boldsymbol{\Omega}_A$ which can be integrated to obtain $\boldsymbol{R}_A$. Since $\boldsymbol{R}_V$ is known, (3.14) and (3.15) are relations between known and estimated quantities and serve as checks on our estimator.

3.4 Estimation of $\boldsymbol{\Omega}_V$

Equation (3.12) require the estimate of $\boldsymbol{\Omega}_V$. Since $\boldsymbol{R}_V$ is differentiable everywhere except at the boundary, $\boldsymbol{\Omega}_V$ will be a smooth function with discontinuities at the boundary. To satisfy the constraint $\boldsymbol{v}_e = \boldsymbol{R}_V\boldsymbol{v}$, $\boldsymbol{v}$ will be the row corresponding to $\boldsymbol{v}_e$ in $\boldsymbol{R}_V$. Hence, this row can be differentiated since it is available directly from the measurement. Thus, components of $\boldsymbol{\Omega}_V$ not along $\boldsymbol{v}_e$ can be determined using relations derived from the row-wise analysis of $\hat{\boldsymbol{\Omega}}$. For the framework specified in Section 3.1, this translates to the determination of $\boldsymbol{e}_1^\top\boldsymbol{\Omega}_V$ and $\boldsymbol{e}_2^\top\boldsymbol{\Omega}_V$.

$$\boldsymbol{e}_1^\top\boldsymbol{\Omega}_V = \dot{\boldsymbol{r}}_3\boldsymbol{r}_2 = -\dot{\boldsymbol{a}}\boldsymbol{r}_2$$
$$\boldsymbol{e}_2^\top\boldsymbol{\Omega}_V = -\dot{\boldsymbol{r}}_3\boldsymbol{r}_1 = \dot{\boldsymbol{a}}\boldsymbol{r}_1$$

Shuster discusses the derivative of the attitude in [9] and demonstrates that the derivative of the rows $\boldsymbol{r}_i$ of the rotation matrix can be written as

$$\dot{\boldsymbol{r}}_i = \boldsymbol{r}_i \times \boldsymbol{\omega}. \tag{3.16}$$

Since the third row of $\boldsymbol{R}_V$ corresponds to $-\boldsymbol{a}$ in the framework discussed in Section 3.1,

$$\dot{\boldsymbol{a}} = -\dot{\boldsymbol{r}}_3 = \boldsymbol{a} \times \boldsymbol{\omega}$$

On the other hand, the determination of $\boldsymbol{e}_3^\top\boldsymbol{\Omega}_V$ requires the time-derivative of the estimates of $\boldsymbol{r}_1$ or $\boldsymbol{r}_2$, which will be not accurate. But, since $\boldsymbol{R}_V$ is known analytically, $\boldsymbol{e}_3^\top\boldsymbol{\Omega}_V$ can be obtained from the simplification of the expression $\boldsymbol{e}_3^\top\boldsymbol{\Omega}_V = \dot{\boldsymbol{r}}_2^\top\boldsymbol{r}_1$ to get an expression in terms of $\boldsymbol{a}$ and $\dot{\boldsymbol{a}}$,

$$\boldsymbol{e}_3^\top\boldsymbol{\Omega}_V = \begin{cases} \dfrac{a_x\dot{a}_y - a_y\dot{a}_x}{1-a_z} & |\theta| \leq \theta_t \\ \dfrac{a_x(a_y\dot{a}_z - a_z\dot{a}_y)}{1-a_x^2} & |\theta| \geq \theta_t. \end{cases} \tag{3.17}$$

The knowledge of $\boldsymbol{\Omega}_V$, specifically $\boldsymbol{e}_3^\top\boldsymbol{\Omega}_V$, completes the complete attitude determination. We pause here to note that, for a general setting, determination of $\boldsymbol{\Omega}_A$ requires the knowledge of $\boldsymbol{\Omega}_V$ along the axis assigned to $\boldsymbol{v}_e$ and follow (3.5) to include $\boldsymbol{R}_I$

and $\boldsymbol{R}_B$.

3.5 Reduced attitude estimate from DAESR

Some of the dynamical systems have constrained degrees of rotational freedom. For example, Mobile Inverted Pendulum do not have roll dynamics [17]. For systems which have dormant roll-dynamics, using the framework specified in Subsection 3.1, $\boldsymbol{a}$ is constrained in one of the coordinate planes passing through the axis of the body frame $\mathbb{G}$ corresponding to $\boldsymbol{e}_3$. Hence, $\boldsymbol{R}_{\boldsymbol{z}}(\psi) = \boldsymbol{I}_3$. This relation is true even if pitch is the constrained degree-of-freedom instead of roll. For such systems, α becomes yaw and the estimator gives an accurate reduced attitude description of the body [18]. On the other hand, if yaw is the constrained degree-of-freedom, then the reduced attitude estimate coincides with the complete attitude estimate since $\dot{\alpha} = 0$. Generalizing from this discussion, we can say for systems which have at least one constrained degree of rotational freedom, DAESR provides an accurate estimate of the reduced attitude. In a general setting, α is not equal to any of the Euler angles as seen in Section 3.2.

3.6 DAESR with non-constant $\boldsymbol{R}_I$

In certain applications, it might be difficult to obtain a vector information which is constant in the inertial frame of interest $\{\mathbb{I}_0\}$. When utilizing magnetometer readings on spherical robots, we know that magnetic field can vary spatially because of the environment. In this section, we generalize DAESR to include vector informations which have a non-constant description in $\{\mathbb{I}_0\}$ and thus obtain the orientation of the body frame $\{\mathbb{B}\}$ with respect to $\{\mathbb{I}\}$. The input set now becomes a single vector information, rate gyros readings and the description of the vector $\boldsymbol{v}_e$ in $\{\mathbb{I}_0\}$.

Since $\boldsymbol{v}_e$ is no longer a constant vector in $\{\mathbb{I}_0\}$, $\boldsymbol{R}_I$ will not be a constant rotation matrix. We use DAESR to denote this non-constant matrix $\boldsymbol{R}_I$.

From (3.1) and (3.5),

$$\begin{aligned}\boldsymbol{R} = \boldsymbol{R}_B^{I_0} &= \boldsymbol{R}_I^{I_0}\boldsymbol{R}_{I_1}^{I}\boldsymbol{R}_G^{I_1}\boldsymbol{R}_B^{G} \\ &= \boldsymbol{R}_I\boldsymbol{R}_{\boldsymbol{v}_e}(\alpha)\boldsymbol{R}_{\boldsymbol{v}\to\boldsymbol{v}_e}\boldsymbol{R}_B \\ &= \boldsymbol{R}_I\boldsymbol{R}_A\boldsymbol{R}_V\boldsymbol{R}_B \\ &= \boldsymbol{R}_{A'}\boldsymbol{R}_{V'}\boldsymbol{R}_A\boldsymbol{R}_V\boldsymbol{R}_B \qquad (\boldsymbol{R}_I = \boldsymbol{R}_{A'}\boldsymbol{R}_{V'}).\end{aligned}$$

We already know that the axis of $\boldsymbol{R}_A$ is along $\boldsymbol{v}_e$ and axis of $\boldsymbol{R}_{A'}$ along the axis of $\{\mathbb{I}_0\}$ corresponding to $\boldsymbol{v}_e$, say $\boldsymbol{e}'$. The knowledge of the description of $\boldsymbol{v}_e$ in $\{\mathbb{I}_0\}$ determines $R_{V'}$. By definition, for some $\alpha', \theta' \in S^1$,

$$\begin{aligned}\boldsymbol{e}' &= R_{V'}\boldsymbol{v}_e \\ \boldsymbol{R}_A &= \boldsymbol{R}_{\boldsymbol{v}_e}(\alpha') \\ \boldsymbol{R}_{A'} &= \boldsymbol{R}_{\boldsymbol{e}'}(\theta').\end{aligned}$$

Using these definitions, we can say that,

$$\begin{aligned}\boldsymbol{R}_{A'}\boldsymbol{R}_{V'}\boldsymbol{R}_A &= \boldsymbol{R}_{\boldsymbol{e}'}(\theta')\boldsymbol{R}_{V'}\boldsymbol{R}_{\boldsymbol{v}_e}(\alpha') \\ &= \boldsymbol{R}_{\boldsymbol{e}'}(\theta'+\alpha')\boldsymbol{R}_{V'}\end{aligned}$$

This helps to rewrite (3.12) as

$$\begin{aligned}\boldsymbol{R}_{V'}\boldsymbol{R}_V\boldsymbol{\omega} &= \boldsymbol{R}_{V'}\boldsymbol{\Omega}_A + \boldsymbol{R}_{V'}\boldsymbol{\Omega}_V \\ &= \boldsymbol{\Omega}_{A'} + \boldsymbol{R}_{V'}\boldsymbol{\Omega}_V\end{aligned}$$

Discussions in Sections 3.3 and 3.4 can be extended to complete the attitude estimation for the generalized DAESR.

3.7 Analysis of strengths and weaknesses in DAESR

With DAESR algorithm discussed completely, we now analyze the strengths and weaknesses in this algorithm.

DAESR algorithm provides a complete attitude estimate from a single vector information and rate gyros readings. The choice of vector information is expanded to encompass any vector described in $\{\mathbb{I}_0\}$ detectable as a vector in $\{\mathbb{B}\}$ with the discussion in Section 3.6. The estimate, owing to its deterministic approach, has a minimal dependence on the previous orientation of the rigid body and respects all the properties of the rotation matrix. It is computationally efficient and can serve as a standalone estimator or as an initial guess for optimal algorithms.

As weaknesses, DAESR is more sensitive to sensor noise as compared to optimal algorithms since it is a deterministic algorithm. When the estimated attitude is differentiated, the sensitivity to sensor noise results in an erroneous differentiation. Apart from this, DAESR involves an integration step. Even though the robustness of the integration step has been demonstrated in the experiments conducted in Chapter 5, the drift in the attitude estimation is inevitable for long runs. The estimation of $\dot{\boldsymbol{v}}$ is essential for Sections 3.3 and 3.4. While an analytical expression for $\dot{\boldsymbol{v}}$ is available, as demonstrated in Section 4.3, the estimation is not immune to sensor measurement noise. The heavy reliance on the estimation of $\dot{\boldsymbol{v}}$ introduces errors in the estimate of attitude.

We now summarize the discussion on DAESR as Algorithm 2. We will be using the framework discussed in Section 3.1. The integration step is done using Euler method for integration. Other methods of integration can be explored for better accuracy [21]. The algorithm requires the following definitions:

1. $\cos\theta_t = \cos(\theta_t = \frac{2\pi}{3})$
2. $\boldsymbol{R}_C = \boldsymbol{I}_3$
3. $\alpha = d\alpha_{\text{prev}} = 0$
4. $d\alpha_{\text{min}}$ defined based on sensor least count
5. $\boldsymbol{R}_I, \boldsymbol{R}_B$ defined based on the system configurations
6. $[\boldsymbol{R}_C, \alpha]$ is updated on every iteration

This section culminates the discussion on DAESR. Next, we will analyze various sources of error and their influence on the estimator followed by the experimental validation.

Algorithm 2 Description of DAESR for framework defined in Section 3.1

procedure DAESR($\boldsymbol{a}, \boldsymbol{a}_{\text{prev}}, \boldsymbol{\omega}, h, \boldsymbol{R}_C, \alpha$)
  $\cos\theta \leftarrow -\boldsymbol{a}[3]$ ▷ Evaluating $-\boldsymbol{a}.\boldsymbol{e}_3$
  $\cos\theta_{\text{prev}} \leftarrow -\boldsymbol{a}_{\text{prev}}[3]$ ▷ Evaluating $-\boldsymbol{a}_{\text{prev}}.\boldsymbol{e}_3$
  if $\cos\theta \geq \cos\theta_t$ **then** ▷ $\theta \in S_L$
    $\boldsymbol{R}_V \leftarrow RvRodriguez(\boldsymbol{a}, -\boldsymbol{e}_3)$ ▷ From Algorithm 1
    $\Omega vz \leftarrow \boldsymbol{e}_3^\top \boldsymbol{\Omega}_V$ ▷ From Eq. (3.17) with $\theta \in S_L$
    if $\cos\theta_{\text{prev}} \leq \cos\theta_t$ **then** ▷ Crossing θ_t, Upper to Lower
      $\boldsymbol{R}_e \leftarrow \boldsymbol{R_y}(\delta)\boldsymbol{R_x}(\gamma)$ ▷ From Eq. (3.6)
      $\Omega vz \leftarrow \boldsymbol{e}_3^\top \boldsymbol{\Omega}_V$ ▷ From Eq. (3.17) with $\theta \in S_U$
      $\boldsymbol{\Omega_G} \leftarrow \boldsymbol{R}_e\, \boldsymbol{\omega}$
      $d\alpha \leftarrow (\boldsymbol{\Omega_G}[3] - \Omega vz)h$ ▷ From Eq. (3.13)
      if $d\alpha \geq d\alpha_{\text{min}}$ **then**
        $\alpha \leftarrow \alpha + d\alpha$ ▷ Euler's method of integration
      end if
      $\boldsymbol{R}_a \leftarrow \boldsymbol{R_z}(\alpha)$
      $\boldsymbol{R}_{\text{est}} \leftarrow \boldsymbol{R}_a\, \boldsymbol{R}_C\, \boldsymbol{R}_e$ ▷ From Eq. (3.5)
      $\boldsymbol{R}_C \leftarrow \boldsymbol{R}_{\text{est}} \boldsymbol{R}_V^\top$ ▷ From Eq. (3.4)
      $\alpha \leftarrow 0$ ▷ Reset α since $\boldsymbol{R}_C$ is updated
      $\boldsymbol{R} \leftarrow \boldsymbol{R}_I\, \boldsymbol{R}_{\text{est}}\, \boldsymbol{R}_B$ ▷ From Eq. (3.5)
      return $[\boldsymbol{R}, \boldsymbol{R}_C, \alpha]$
    end if
  else ▷ $\theta \in S_U$
    $\boldsymbol{R}_V \leftarrow \boldsymbol{R_y}(\delta)\boldsymbol{R_x}(\gamma)$ ▷ From Eq. (3.6)
    $\Omega vz \leftarrow \boldsymbol{e}_3^\top \boldsymbol{\Omega}_V$ ▷ From Eq. (3.17) with $\theta \in S_U$
    if $\cos\theta_{\text{prev}} \geq \cos\theta_t$ **then** ▷ Crossing θ_t, Lower to Upper
      $\boldsymbol{R}_r \leftarrow RvRodriguez(\boldsymbol{a}, -\boldsymbol{e}_3)$
      $\Omega vz \leftarrow \boldsymbol{e}_3^\top \boldsymbol{\Omega}_V$ ▷ From Eq. (3.17) with $\theta \in S_L$
      $\boldsymbol{\Omega_G} \leftarrow \boldsymbol{R}_r\, \boldsymbol{\omega}$
      $d\alpha \leftarrow (\boldsymbol{\Omega_G}[3] - \Omega vz)h$
      if $d\alpha \geq d\alpha_{\text{min}}$ **then**
        $\alpha \leftarrow \alpha + d\alpha$
      end if
      $\boldsymbol{R}_a \leftarrow \boldsymbol{R_z}(\alpha)$ ▷ Here, α is actually $\alpha + \psi$
      $\boldsymbol{R}_{\text{est}} \leftarrow \boldsymbol{R}_a\, \boldsymbol{R}_C\, \boldsymbol{R}_r$ ▷ From Eq. (3.5)
      $\boldsymbol{R}_C \leftarrow \boldsymbol{R}_{\text{est}} \boldsymbol{R}_V^\top$
      $\alpha \leftarrow 0$
      $\boldsymbol{R} \leftarrow \boldsymbol{R}_I\, \boldsymbol{R}_{\text{est}}\, \boldsymbol{R}_B$
      return $[\boldsymbol{R}, \boldsymbol{R}_C, \alpha]$
    end if
  end if
  $\boldsymbol{\Omega_G} \leftarrow \boldsymbol{R}_V\, \boldsymbol{\omega}$
  $d\alpha \leftarrow (\boldsymbol{\Omega_G}[3] - \Omega vz)h$
  if $d\alpha \geq d\alpha_{\text{min}}$ **then**
    $\alpha \leftarrow \alpha + d\alpha$
  end if
  $\boldsymbol{R}_a \leftarrow \boldsymbol{R_z}(\alpha)$
  $\boldsymbol{R} \leftarrow \boldsymbol{R}_I\, \boldsymbol{R}_a\, \boldsymbol{R}_C\, \boldsymbol{R}_V\, \boldsymbol{R}_B$
  return $[\boldsymbol{R}_{\text{est}}, \boldsymbol{R}_C, \alpha]$
end procedure

CHAPTER 4

Analysis of various sources of error in the estimate

The major sources of error for DAESR are:

1. Error in the rate gyro readings
2. Error in the estimate of $\boldsymbol{v}$
3. Error in the estimate of $\dot{\boldsymbol{v}}$
4. Error in the numerical integration of $\dot{\alpha}$

We will now be focussing on the contribution in the error of the estimation of the attitude by the proposed algorithm by these components.

Remark 4.0.1. *In this section, the measured quantities will be denoted by $\tilde{x}$ to distinguish from their theoretical counterparts x. We use Δx to denote the difference between the measurement and the theoretical estimate of a measured quantity. Thus, $\tilde{x} = x + \Delta x$.*

4.1 Error due to rate gyros

Gyroscopes measure the body angular velocity experienced by the object on which it is mounted. The noise present in the rate gyro readings are due to Angular Random Walk (ARW), gyroscopic drift and measurement noise [22]. We assume a simple constant bias model for the error in the rate gyro readings. The constant bias is determined by averaging the rate gyro readings during the time in which the object is motionless. Mahoney, in [10], discusses the extraction of rate gyro biases based on the knowledge of R. We denote the rate gyro reading after compensating for the constant bias as $\tilde{\boldsymbol{\omega}}$.

From (3.5), it is clear that $\boldsymbol{\omega}$ only influences the estimate of $\boldsymbol{R}_A$. (3.13) on using $\tilde{\boldsymbol{\omega}}$ becomes

$$\boldsymbol{e}_3^\top \boldsymbol{\Omega}_A = \boldsymbol{e}_3^\top \left(\boldsymbol{R}_V \boldsymbol{R}_B \left(\boldsymbol{\omega} + \boldsymbol{\Delta\omega}\right)\right) - \boldsymbol{e}_3^\top \boldsymbol{\Omega}_V.$$

Assume $\boldsymbol{R}_A^*$ is the rotation matrix corresponding to the rotation about $\boldsymbol{v}_e$ by an angle equivalent to the time integral of $\boldsymbol{e}_3^\top(\boldsymbol{R}_V\boldsymbol{R}_B\boldsymbol{\Delta\omega})$. On integrating the erroneous $\dot{\alpha}$, $\boldsymbol{R}_A$ becomes $\boldsymbol{R}_A\boldsymbol{R}_A^*$. The error in $\boldsymbol{R}_{\text{est}}$ manifests as $\boldsymbol{R}_{\text{est}}\boldsymbol{R}_{\text{est}}^*$ where

$$\boldsymbol{R}_{\text{est}}^* = \boldsymbol{R}_B^\top\boldsymbol{R}_V^\top\boldsymbol{R}_A^*\boldsymbol{R}_V\boldsymbol{R}_B.$$

For $\frac{|\boldsymbol{\Delta\omega}|}{|\boldsymbol{\omega}|} \ll 1$, $\boldsymbol{R}_A^*$ approaches $\boldsymbol{I}_3$.

4.2 Error in the estimate of $\boldsymbol{v}$

The resolution of the constant vector $\boldsymbol{v}_e$ in the $\{\mathbb{B}\}$ could have errors introduced by sensing. $\boldsymbol{R}_{\text{est}}$ needs to be adjusted to account for this error. If we define $\boldsymbol{R}_{\boldsymbol{v}\to\boldsymbol{v}_e}^*$ as the rotation matrix that rotates vector $\tilde{\boldsymbol{v}}$ to $\boldsymbol{v}$, then (3.5) can be modified as

$$\tilde{\boldsymbol{R}_{\text{est}}} = \boldsymbol{R}_I\boldsymbol{R}_A\boldsymbol{R}_V\boldsymbol{R}_{\boldsymbol{v}\to\boldsymbol{v}_e}^*\boldsymbol{R}_B.$$

While it is clear that for $\boldsymbol{\Delta v} = 0$, $\boldsymbol{R}_{\boldsymbol{v}\to\boldsymbol{v}_e}^* = \boldsymbol{I}_3$, we explore through the following proposition the conditions under which $\boldsymbol{R}_{\boldsymbol{v}\to\boldsymbol{v}_e}^*$ can be approximated as $\boldsymbol{I}_3$.

Proposition 4.2.1. *$\boldsymbol{R}_{\boldsymbol{v}\to\boldsymbol{v}_e}^*$ can be approximated as $\boldsymbol{I}_3$ if $\epsilon \triangleq \frac{|\boldsymbol{\Delta v}|}{|\boldsymbol{v}|} \ll 1$.*

Proof: Based on the discussion in Section 2.1, we have already demonstrated that for rotating $\tilde{\boldsymbol{v}}$ to $\boldsymbol{v}$, if the angle of separation is θ, then

$$\cos\theta = \frac{\boldsymbol{v}.(\tilde{\boldsymbol{v}})}{|\boldsymbol{v}||\tilde{\boldsymbol{v}}|} = \frac{\boldsymbol{v}.(\boldsymbol{v}+\boldsymbol{\Delta v})}{|\boldsymbol{v}||\boldsymbol{v}+\boldsymbol{\Delta v}|} = \frac{|\boldsymbol{v}|^2 + \boldsymbol{v}.\boldsymbol{\Delta v}}{|\boldsymbol{v}||\boldsymbol{v}+\boldsymbol{\Delta v}|} \tag{4.1}$$

But $|\boldsymbol{v}+\boldsymbol{\Delta v}| = \sqrt{|\boldsymbol{v}|^2 + |\boldsymbol{\Delta v}|^2 + 2|\boldsymbol{v}||\boldsymbol{\Delta v}|\cos\phi}$, where ϕ is the angle between $\boldsymbol{\Delta v}$ and $\boldsymbol{v}$ and hence $\cos\phi = \frac{\boldsymbol{\Delta v}.\boldsymbol{v}}{|\boldsymbol{\Delta v}||\boldsymbol{v}|}$. Applying these relations in (4.1), we have

$$\cos\theta = \frac{|\boldsymbol{v}|^2 + |\boldsymbol{v}||\boldsymbol{\Delta v}|\cos\phi}{|\boldsymbol{v}||\boldsymbol{v}+\boldsymbol{\Delta v}|} = \frac{1+\epsilon\cos\phi}{\sqrt{1+\epsilon^2+2\epsilon\cos\phi}}. \tag{4.2}$$

Equation (4.2) proves the claim that for small ϵ, we can approximate $\cos\theta$ as 1 implying $\boldsymbol{R}_{\boldsymbol{v}\to\boldsymbol{v}_e}^*$ as $\boldsymbol{I}_3$. ■

Since $\boldsymbol{\Delta v}$ is generally unknown, Proposition 4.2.1 provide conditions under which the estimator described in (3.5) is valid.

Accelerometers are modelled by the following equation,

$$\boldsymbol{a} = \boldsymbol{R}^\top \boldsymbol{g} + \boldsymbol{a}_b + \boldsymbol{\Delta a}$$

where $\boldsymbol{g} = -\boldsymbol{e}_3$, $\boldsymbol{a}_b$ is the linear acceleration of the body and $\boldsymbol{\Delta a}$ is the additive noise in the measurement. This model is applicable for systems where the $\boldsymbol{z}$-axis of the IMU is pointing downwards.

Hence in the framework defined in Section 3.1, the perturbation $\boldsymbol{\Delta v}$ corresponds to the linear acceleration experienced by the object and the additive noise to the measurement. The Proposition 4.2.1, thus, suggests that accelerometers can be used as the vector correspondence, provided the linear acceleration of the body and the additive noise is much smaller in magnitude than the acceleration due to gravity.

4.3 Error analysis for the estimation of $\dot{\boldsymbol{v}}$

We use (3.16) to estimate the derivative of a vector $\boldsymbol{v} \in S^2$. The error in this estimate in the presence of additive noise is

$$|\boldsymbol{\Delta \dot{v}}| = |\boldsymbol{\Delta v} \times \boldsymbol{\omega} + \boldsymbol{v} \times \boldsymbol{\Delta w} + \boldsymbol{\Delta v} \times \boldsymbol{\Delta \omega}|$$

which is independent of sampling frequency and depends only on the measurement noise.

In Appendix A, we discuss an approximate method to estimate $\dot{\boldsymbol{v}}$. First-difference based definition of the derivative leads to an error of order $O(h^2)$ if h is the sampling time period. This estimation requires normalization of a vector whose length is dependent on the sampling frequency and the trajectory of the vector $\boldsymbol{v}$. Hence, the sampling frequency and the threshold for which the algorithm returns a zero vector as the differentiation needs to be adjusted to the vector dynamics appropriately. Figure A.1 depicts the estimator and the corresponding error.

The theoretical estimate of the norm and the approximate estimate proposed in (A.3)

are compared and the results of the verification can be seen in Figure A.2.

4.4 Error in the numerical integration of $\dot{\alpha}$

The numerical integration for estimation of complete attitude is done using the Euler's method of integration. If we define h as the sampling time period, then this method of integration has an error of estimate in the order of $O(h^2)$.

CHAPTER 5

Experimental Validation

The experimental validation of DAESR was done on three different existing laboratory setups:

1. Twin Rotor Multiple-Input Multiple-Output System
2. Spherical Robot
3. Mobile Inverted Pendulum

The experiments on Twin Rotor MIMO system required the development of a printed circuit board for the data acquisition and processing. Figure 5.1 shows the PCB developed for the experimental setup at Dynamics and Control Lab, IIT Madras.

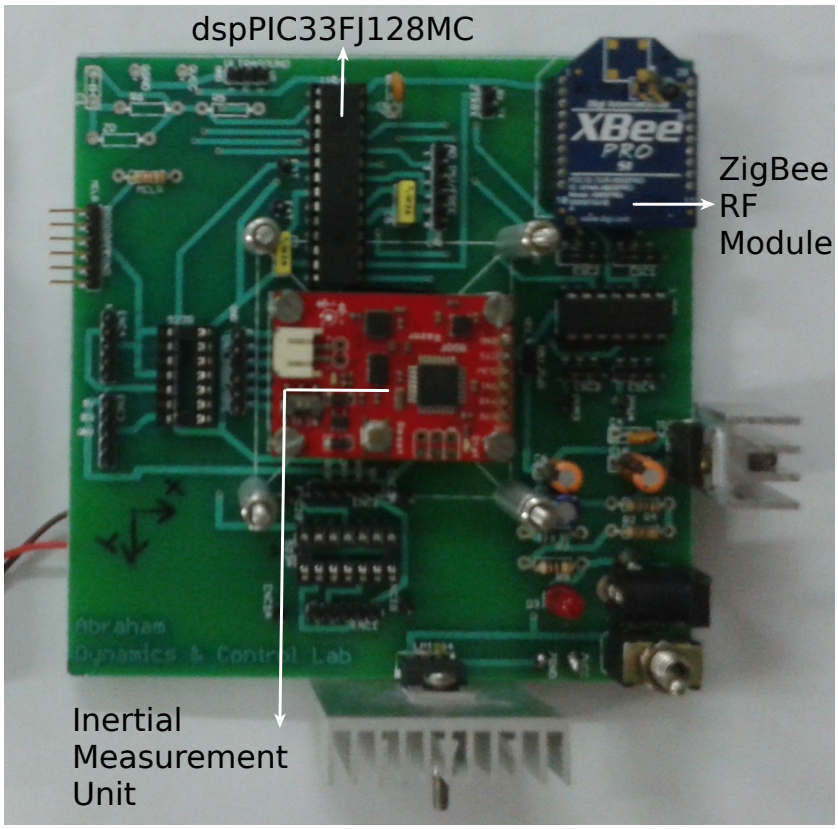

Figure 5.1: Printed Circuit Board developed for the experimental setup

5.1 Twin Rotor MIMO System

The twin rotor multiple-input multiple-output system, as shown in Figure 5.2, is a mechanical system with two links, a horizontal link connected to the base through a rotational joint and a link perpendicular to the horizontal link connected through another rotational joint with propellers attached at both ends.

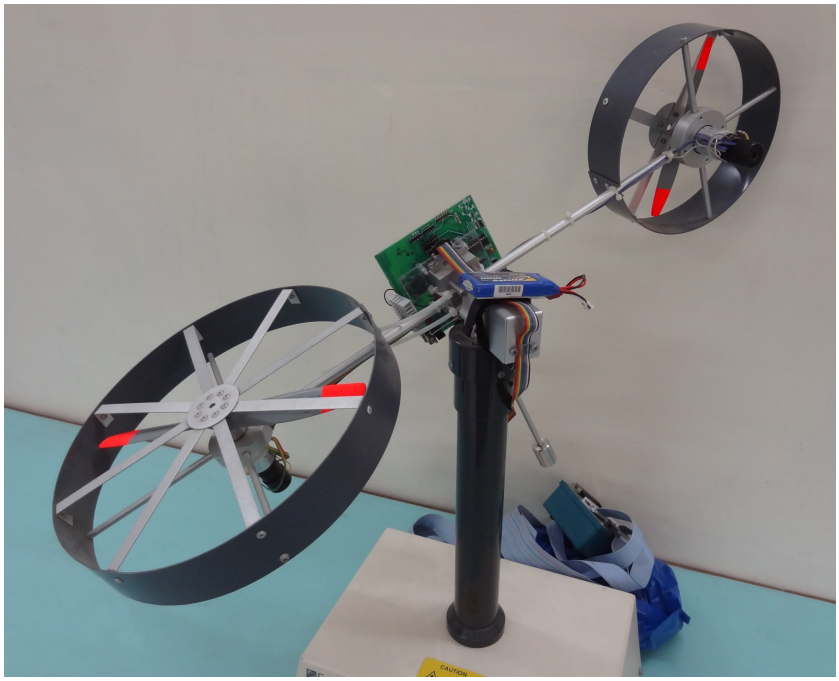

Figure 5.2: Experimental Setup for the Twin Rotor MIMO System

The PCB with the Inertial Measurement Unit (IMU) is mounted on the pivot point as demonstrated in Figure 5.2. In this configuration, the IMU experiences minimal linear acceleration. The accelerometer readings can, thus, be approximated as the true resolution of gravity in the body frame $\{\mathbb{G}\}$. The framework described in Section 3.1 is used for the experimental validation and $\boldsymbol{R}_I = \boldsymbol{I}_3$. Due to the system configuration, $\boldsymbol{R}_B = \boldsymbol{R}_y(\frac{\pi}{2})$. As mentioned in Section 3.2, owing to zero-roll dynamics, α is the yaw angle in ZYX convention. This also shows that the estimate for $\dot{\alpha}$ and the estimate for $\boldsymbol{R}_V$ forms the reduced attitude estimate for the system as discussed in Section 3.5.

The IMU used for this experiment is a low-cost Sparkfun 9 Degrees-of-Freedom - Razor IMU (SEN-10736) [23]. The accelerometer and rate gyro readouts are obtained from the IMU at 100 Hz. The rate gyro on SEN-10736 is an InvenSense ITG-3200 which has a settling time of 50 ms. At the commencement of experiments, the rate gyro

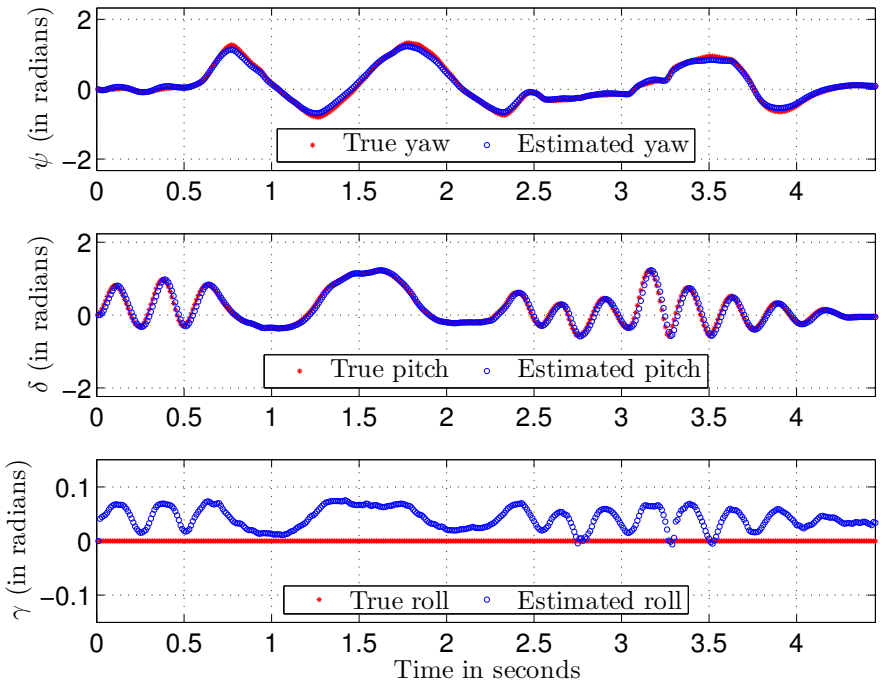

Figure 5.3: Comparison plot of Euler angles (ψ, δ, γ) with truth value from encoders. Iteration 1 in Table 5.1.

readouts were continuously monitored and allowed to stabilize to an approximately constant bias which was extracted and subtracted from the subsequent readouts. In order to eliminate the higher frequency noises picked by the rate gyro and accelerometers, the signals are filtered using a type-II Chebyshev filter. The filter is a second-order filter with a notch at 22.5 Hz and the stopband ripple 60 dB below the peak passband value.

The truth value of yaw and pitch are obtained from the decomposition of the rotation matrix obtained using the encoders. It is compared with the estimated values and the results are presented in Figure 5.3. It should be noted that the estimate for yaw is obtained by numerical integrating the estimate of $\dot{\alpha}$ from (3.13). The robustness of the reduced attitude estimate was demonstrated by repeating the experiment. The results are tabulated in Table 5.1. The roll estimate is very close to the true roll of the system which is zero.

Iteration	Maximum Absolute Error (in radians)		RMS Error (in radians)		Correlation Percentage	
	Yaw	Pitch	Yaw	Pitch	Yaw	Pitch
1	0.1330	0.1157	0.0627	0.0011	99.53	99.66
2	0.1869	0.1740	0.0620	0.0011	99.40	98.92
3	0.1775	0.0993	0.0838	0.0015	99.23	99.53
4	0.1805	0.1316	0.0737	0.0013	99.66	99.51
5	0.1389	0.1497	0.0684	0.0012	99.06	99.17

Table 5.1: Errors between estimated yaw and pitch and the truth values quantified using various figures of merit.

5.2 Spherical Robot

Figure 5.4: Experimental Setup for the Spherical Robot

The spherical robot developed at Dynamics and Control Lab, IIT Madras is shown in Figure 5.4. All the hardware is enclosed in a spherical acrylic shell composed of two detachable hemispheres. The internal hardware is supported on an endoskeleton consisting three orthogonal rings and a crossbeam. The crossbeam is used to place the IMU at the center of the robot. The IMU used is the Analog devices ADIS16400. It has a 3-DOF rate gyro, 3-DOF accelerometer and 3-DOF magnetometer. The dsPIC microcontroller is used for motor control, reading sensors and PC communication using Xbee module.

The spherical bot was rolled on two paths - *circular* and *trifolium* trajectory. Indepth robustness analysis is done for the circular path using the constraint $x^2+y^2 = c^2$, where $c = 1.25$ m is the radius of the circular trajectory. Utilizing the non-holonomic con-

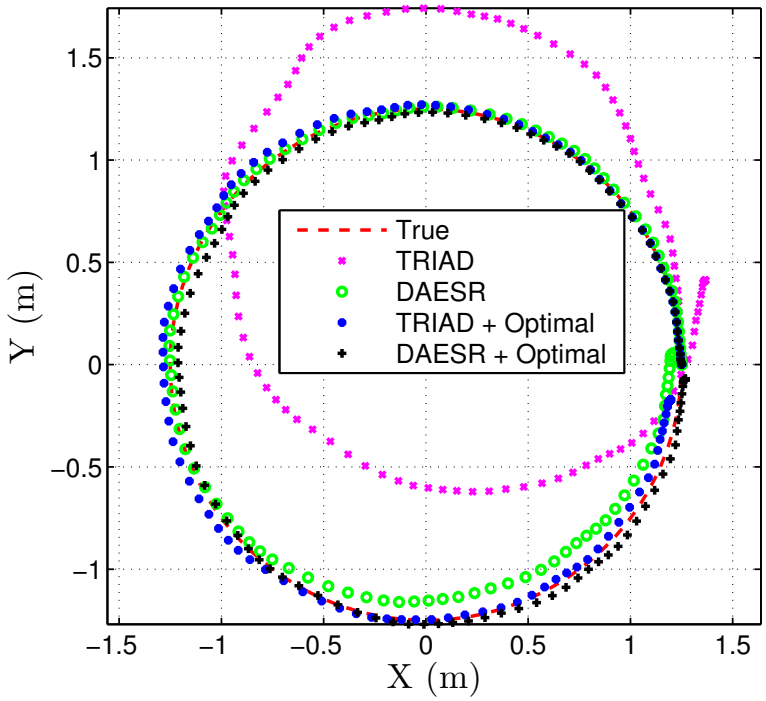

Figure 5.5: Spherical robot dead-reckoning - Circular Trajectory - Iteration 5 in Tables 5.2, 5.3 and 5.4.

straints governing the dynamics, we can get a deterministic estimate of the translational velocity ($\boldsymbol{v}_{\text{in}}$) of the spherical bot of radius r,

$$\boldsymbol{e}_1^\top \boldsymbol{v}_{\text{in}} = -r\boldsymbol{e}_2^\top \boldsymbol{\Omega} = -r\boldsymbol{r}_2.\boldsymbol{\omega}$$
$$\boldsymbol{e}_2^\top \boldsymbol{v}_{\text{in}} = r\boldsymbol{e}_1^\top \boldsymbol{\Omega} = r\boldsymbol{r}_1.\boldsymbol{\omega}.$$

In Table 5.3, $\boldsymbol{R}_D$ and $\boldsymbol{R}_T$ correspond to attitude estimations from DAESR and TRIAD whereas $\boldsymbol{R}_{DO}$ and $\boldsymbol{R}_{TO}$ correspond to optimal attitude estimation using Mahoney's complimentary filter using DAESR and TRIAD as initial guesses respectively.

Another figure of merit is to measure $|(\boldsymbol{R}_{\text{est}}^\top \dot{\boldsymbol{R}}_{\text{est}})^\vee - \boldsymbol{\omega}|$. Since deterministic algorithms do not perform an incremental adjustment over the previous estimates, estimates of the derivative of $\boldsymbol{R}_{\text{est}}$ using the approximate method discussed in Appendix A is much less accurate as compared to the optimal algorithms. This weakness of the deterministic algorithms is observed in the column of maximum deviation in Table 5.4. Hence, the deterministic algorithms and their optimal counterparts are compared separately in Figure 5.7. We also note that the best estimate for $\dot{\boldsymbol{R}}_{\text{est}}$ is $\boldsymbol{R}_{\text{est}}\hat{\boldsymbol{\omega}}$.

Iteration	Algorithm	Maximum Absolute Error (in m)	RMS Error (in m)	Final Offset(in m)
1	TRIAD	0.5855	0.3471	0.2215
	DAESR	0.2878	0.2100	0.1258
	TRIAD+Optimal	0.2591	0.2131	0.0366
	DAESR+Optimal	0.2765	0.2056	0.0992
2	TRIAD	0.5355	0.3048	0.0858
	DAESR	0.3678	0.2459	0.1238
	TRIAD+Optimal	0.2718	0.2357	0.1053
	DAESR+Optimal	0.2762	0.2134	0.1294
3	TRIAD	0.5755	0.3549	0.6234
	DAESR	0.4734	0.3023	0.3955
	TRIAD+Optimal	0.2882	0.2585	0.1126
	DAESR+Optimal	0.3574	0.2604	0.1306
4	TRIAD	0.5338	0.3233	0.3071
	DAESR	0.3886	0.2589	0.1369
	TRIAD+Optimal	0.7072	0.4080	0.1627
	DAESR+Optimal	0.6001	0.3550	0.2020
5	TRIAD	0.7425	0.4213	0.4293
	DAESR	0.3582	0.2357	0.1218
	TRIAD+Optimal	0.3000	0.2516	0.1787
	DAESR+Optimal	0.2847	0.2501	0.0970

Table 5.2: Robustness analysis of dead-reckoning using attitude information - Circular Trajectory.

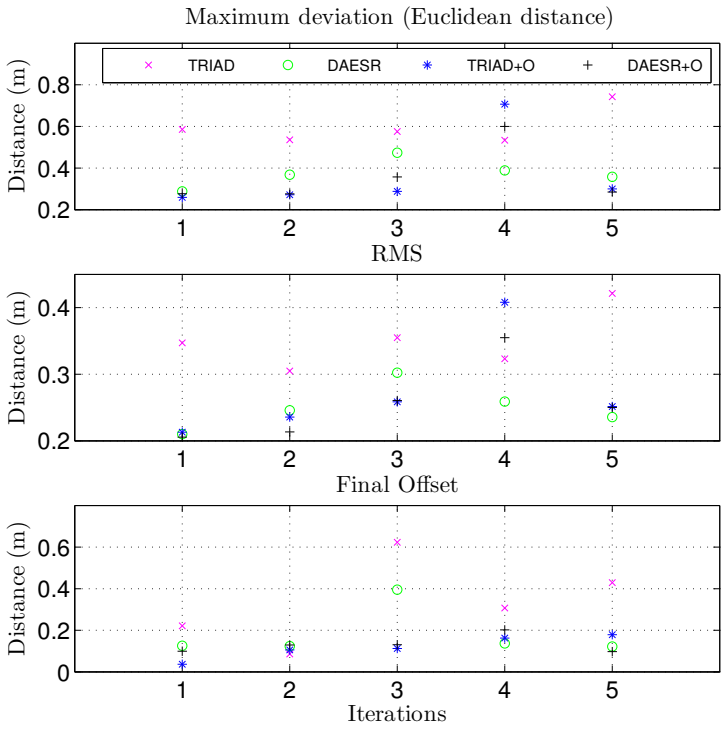

Figure 5.6: Visualization of Table 5.2. The legend of the first subplot carries forward to the second and third subplots.

Iteration	Figure of Merit	$\frac{\mathrm{tr}(\boldsymbol{R}_D^\top \boldsymbol{R}_T)-1}{2}$	$\frac{\mathrm{tr}(\boldsymbol{R}_D^\top \boldsymbol{R}_{TO})-1}{2}$	$\frac{\mathrm{tr}(\boldsymbol{R}_D^\top \boldsymbol{R}_{DO})-1}{2}$	$\frac{\mathrm{tr}(\boldsymbol{R}_{DO}^\top \boldsymbol{R}_T)-1}{2}$	$\frac{\mathrm{tr}(\boldsymbol{R}_{DO}^\top \boldsymbol{R}_{TO})-1}{2}$
1	Max Diff	0.2221	0.02353	0.01796	0.2416	0.01047
	RMS	0.05135	0.00559	0.002928	0.06278	0.005695
2	Max Diff	0.2425	0.0302	0.03448	0.2514	0.02628
	RMS	0.07188	0.0107	0.002753	0.07728	0.01069
3	Max Diff	0.2238	0.0478	0.04858	0.2559	0.00162
	RMS	0.04119	0.01276	0.01671	0.06152	0.0007638
4	Max Diff	0.2381	0.1066	0.08649	0.1621	0.01351
	RMS	0.05498	0.05416	0.03487	0.03085	0.007487
5	Max Diff	0.1402	0.02466	0.02735	0.2124	0.003157
	RMS	0.03151	0.00966	0.008994	0.05301	0.00201

Table 5.3: Analysis of offset across various attitude estimation - Circular Trajectory. $\mathrm{tr}(\boldsymbol{A})$ refers to the trace of $\boldsymbol{A}$.

Iteration	Algorithm	Maximum Absolute Error (in radians/s)	RMS Error (in radians/s)
1	TRIAD	5.689	0.8903
	DAESR	5.291	0.7872
	TRIAD+Optimal	0.2381	0.05124
	DAESR+Optimal	0.2337	0.049
2	TRIAD	3.798	0.8529
	DAESR	5.454	0.8358
	TRIAD+Optimal	0.2604	0.0552
	DAESR+Optimal	0.2583	0.05337
3	TRIAD	4.343	0.8607
	DAESR	5.529	0.858
	TRIAD+Optimal	0.3111	0.06252
	DAESR+Optimal	0.3169	0.06174
4	TRIAD	9.045	0.9566
	DAESR	7.258	0.9451
	TRIAD+Optimal	0.3445	0.06339
	DAESR+Optimal	0.3339	0.06442
5	TRIAD	1.804	0.5329
	DAESR	1.765	0.463
	TRIAD+Optimal	0.155	0.07462
	DAESR+Optimal	0.1589	0.07469

Table 5.4: Comparison of the figure of merit $|(\boldsymbol{R}_{\text{est}}^\top \dot{\boldsymbol{R}}_{\text{est}})^\vee - \boldsymbol{\omega}|$ - Circular Trajectory.

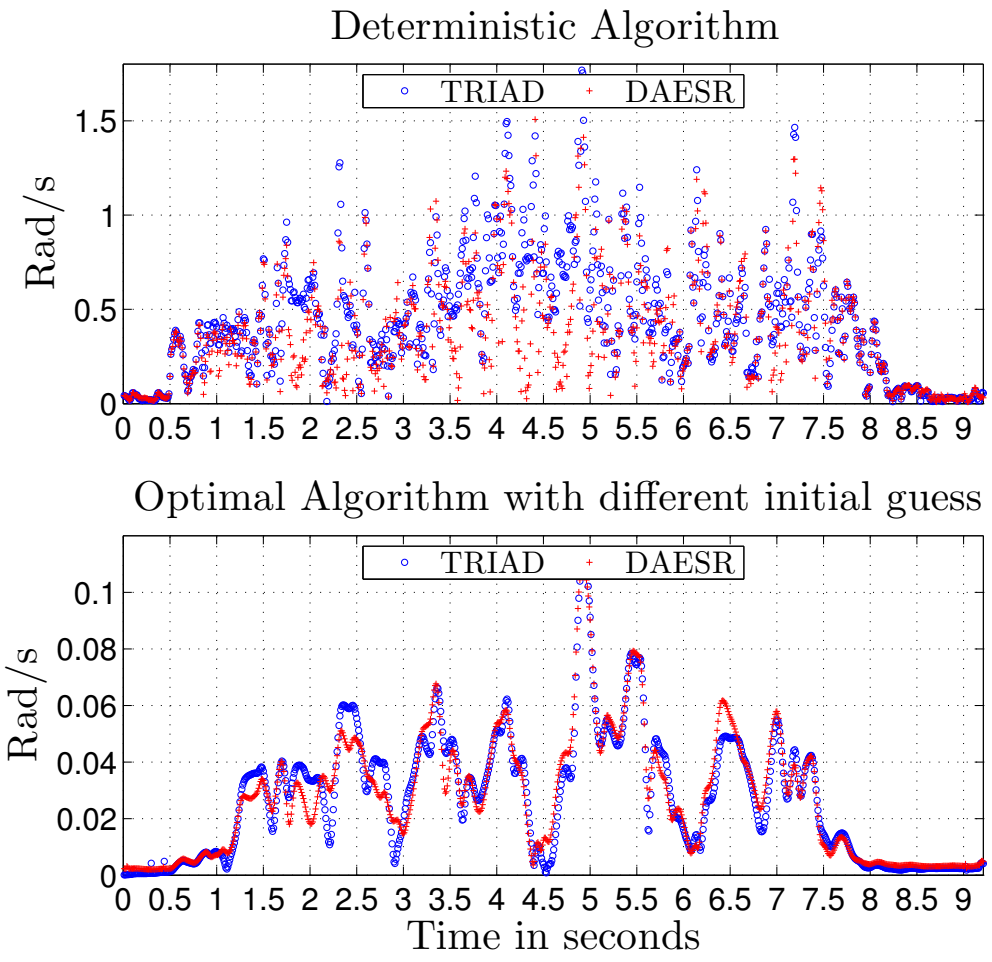

Figure 5.7: Comparison of the figure of merit $|(\boldsymbol{R}_{\text{est}}^{\top}\dot{\boldsymbol{R}}_{\text{est}})^{\vee} - \boldsymbol{\omega}|$ - Circular Trajectory. Iteration 5 in Table 5.4.

Iteration	Figure of Merit	$\frac{\text{tr}(\boldsymbol{R}_D^{\top}\boldsymbol{R}_T)-1}{2}$	$\frac{\text{tr}(\boldsymbol{R}_D^{\top}\boldsymbol{R}_{TO})-1}{2}$	$\frac{\text{tr}(\boldsymbol{R}_D^{\top}\boldsymbol{R}_{DO})-1}{2}$	$\frac{\text{tr}(\boldsymbol{R}_{DO}^{\top}\boldsymbol{R}_T)-1}{2}$	$\frac{\text{tr}(\boldsymbol{R}_{DO}^{\top}\boldsymbol{R}_{TO})-1}{2}$
1	Max Diff	0.252	0.1808	0.07252	0.1815	0.03795
	RMS	0.07953	0.06189	0.02108	0.04389	0.02205
2	Max Diff	0.3421	0.1281	0.03575	0.2232	0.0487
	RMS	0.09132	0.04541	0.007388	0.06192	0.01906
3	Max Diff	0.4169	0.1192	0.04019	0.276	0.04404
	RMS	0.09353	0.04864	0.01109	0.05786	0.01749
4	Max Diff	0.3291	0.12	0.07484	0.2359	0.03794
	RMS	0.08262	0.04729	0.0116	0.0526	0.01839
5	Max Diff	0.1018	0.05017	0.02982	0.09122	0.01127
	RMS	0.02967	0.01479	0.006991	0.02587	0.00657

Table 5.5: Analysis of offset across various attitude estimation - Trifolium Trajectory. $\text{tr}(\boldsymbol{A})$ refers to the trace of $\boldsymbol{A}$.

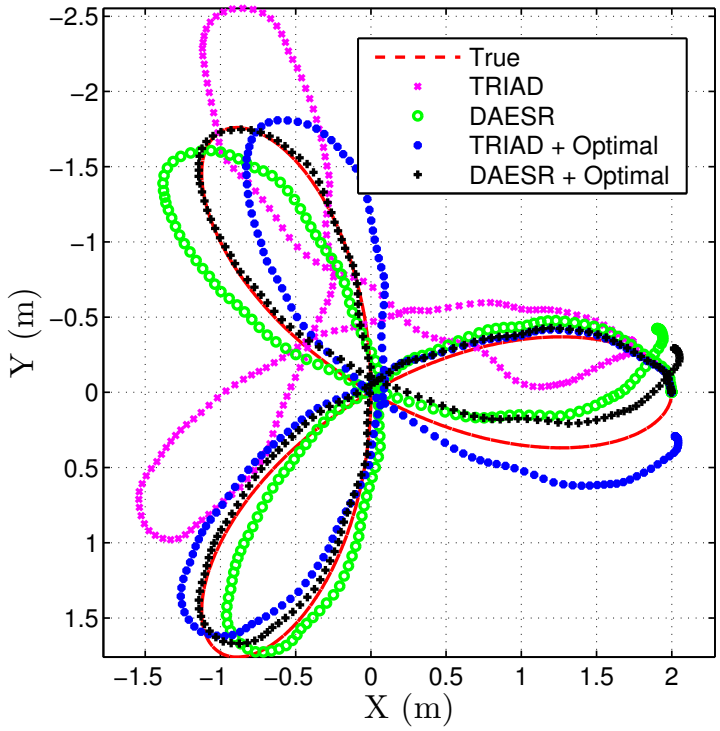

Figure 5.8: Spherical robot dead-reckoning - Trifolium Trajectory. Iteration 4 in Tables 5.5 and 5.6.

Iteration	Algorithm	Maximum Absolute Error (in radians/s)	RMS Error (in radians/s)
1	TRIAD	6.382	0.9533
	DAESR	9.46	0.9251
	TRIAD+Optimal	0.4867	0.06655
	DAESR+Optimal	0.4612	0.06607
2	TRIAD	6.071	0.969
	DAESR	9.01	1.007
	TRIAD+Optimal	0.2843	0.061
	DAESR+Optimal	0.2877	0.06068
3	TRIAD	8.522	1.18
	DAESR	8.466	1.163
	TRIAD+Optimal	0.3652	0.06842
	DAESR+Optimal	0.354	0.06848
4	TRIAD	6.98	1.077
	DAESR	8.293	1.132
	TRIAD+Optimal	0.3616	0.07515
	DAESR+Optimal	0.3564	0.07545
5	TRIAD	1.451	0.4449
	DAESR	1.449	0.4258
	TRIAD+Optimal	0.1621	0.06467
	DAESR+Optimal	0.1616	0.06457

Table 5.6: Comparison of the figure of merit $|(\boldsymbol{R}_{\text{est}}^{\top}\dot{\boldsymbol{R}}_{\text{est}})^{\vee} - \boldsymbol{\omega}|$ - Trifolium Trajectory.

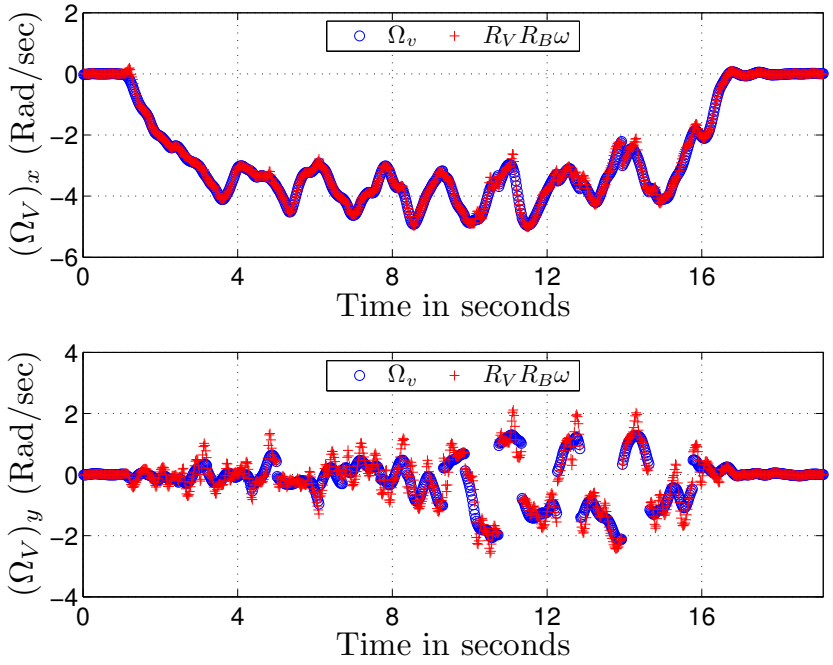

Figure 5.9: Logical Checks on the estimator as given by (3.14) and (3.15) - Circular Trajectory. Iteration 5 in Table 5.4

Figure 5.5 and 5.8 demonstrates the performance of the algorithm for standalone attitude determination and as the initial guess for an optimal algorithm. The minimal final offset seen in both the trajectory suggests low accumulation of error in the attitude estimation as seen in Table 5.2. Tables 5.3, 5.4, 5.5 and 5.6 further validate the robustness and the accuracy of the algorithm. The nonlinear complimentary filter based algorithm for estimation of attitude proposed by Mahoney [10] was used as the optimal algorithm to compare the performance. When DAESR is used as the initial guess for the optimal algorithm, the dead-reckoning was found to be most accurate.

The checks obtained in (3.14) and (3.15) are plotted in Figure 5.9 which were obtained while the spherical bot traced a circle. As expected from the discussion in Section 3.4, the discontinuities appear in Ω_V at $\theta = \theta_t$.

5.3 Mobile Inverted Pendulum

The MIP setup, NIDOLA, developed at the Dynamics and Control Laboratory, IITM is shown in Figure 5.10. The main sensor is a digital six degree-of-freedom IMU (ADIS16354) which has a 3-DOF rate gyro and 3-DOF accelerometer. The calcula-

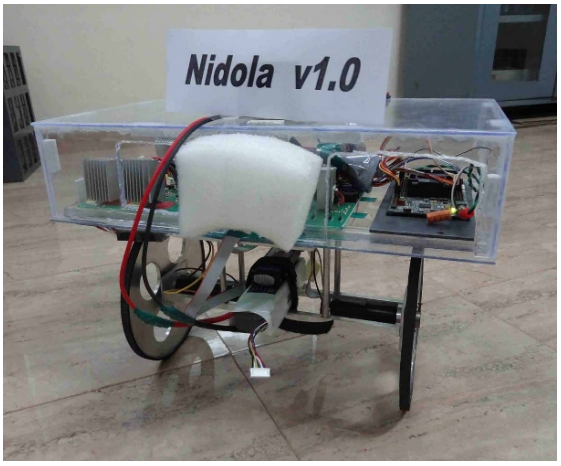

Figure 5.10: Experimental Setup for the Mobile Inverted Pendulum

tion of (x, y) can be performed through dead reckoning from the information available through the encoders and the IMU. Xbee wireless module is used to transmit all states of the robot for storage in PC. Sensor interface and control computations are performed on a TI DSP board (eZdsp F28335). Second-order low-pass filters are used on all sensor readings and computed derivatives to avoid high frequency noise.

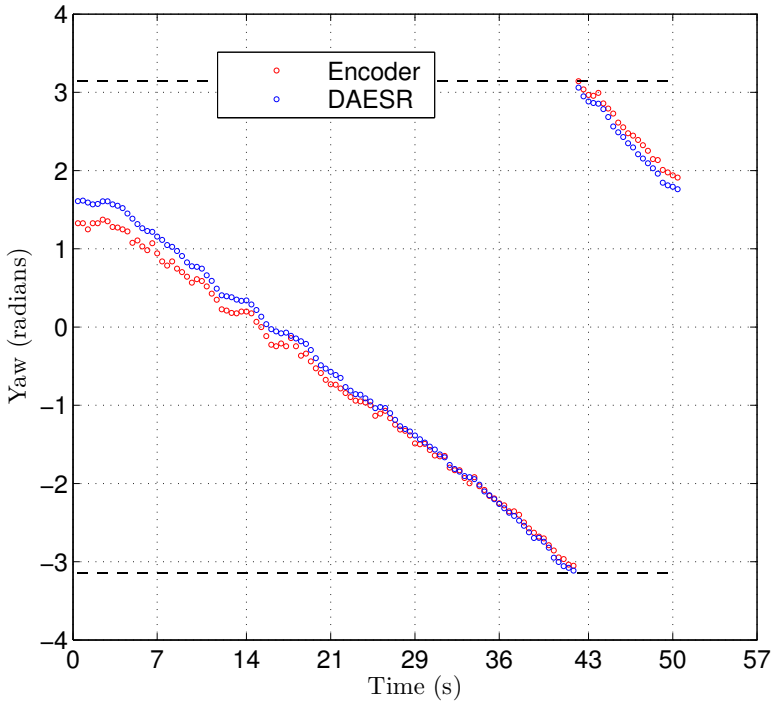

Figure 5.11: Comparison of the yaw estimated using DAESR and the encoder readings

Since the experimental setup has an IMU which does not have a magnetometer, estimation of yaw is not possible using TRIAD or the combination of TRIAD and Ma-

honey's complimentary filter. At this point, owing to its advantage of using a single vector information, DAESR can be utilized to estimate yaw using just the accelerometer and rate gyro readings deterministically. The encoders on the robot's wheels are used to estimate the direction of the heading velocity, a quantity directly related to the yaw of the robot. Figure 5.11 compares the estimated yaw and the truth.

CHAPTER 6

Conclusion

6.1 Summary

This dissertation introduces a computationally inexpensive algorithm to estimate the attitude of an object using just the information obtained from an Inertial Measurement Unit (IMU). The estimator is ensured to have a complete attitude representation. Various sources of error in the estimation was identified and suitable corrections were proposed. The robustness of the algorithm has been analyzed by incorporating figures of merit in three domains - integrated, scalar and differentiated figure of merit. Experimental validation was done using a Twin Rotor MIMO System, a spherical robot and Mobile Inverted Pendulum.

6.2 Concluding remarks

DAESR, as discussed in this dissertation, requires a minimal input set. As demonstrated in Section 5.3, this becomes advantageous in scenarios where enough information for conventional attitude estimators is not available. Also, as mentioned in Section 1.2, DAESR can be used to estimate attitude independent of accelerometer readings allowing for more accurate estimation of translational velocity. No loss in accuracy was observed as compared to TRIAD despite using lesser information.

APPENDIX A

Estimation of derivative of $\boldsymbol{v} \in S^2$ and $\boldsymbol{R} \in \boldsymbol{SO}(3)$

Equation (3.16) gives an analytical expression for obtaining the derivative of a vector $\boldsymbol{v} \in S^2$ when $\boldsymbol{v}$ is the resolution of one of the inertial frame axes $\{\mathbb{I}\}$ in the body frame $\{\mathbb{G}\}$. In situations where analytical expression of the differentiation of a signal is not known, numerical differentiation is generally employed. One of the basic methods to estimate the differentiation of a function at a point without *a priori* explicit knowledge of the signal is to find successive differences and divide it by the sampling time period [21].

While differentiating vectors lying in S^2, an extra constraint needs to be respected,

$$\boldsymbol{v}^\top \dot{\boldsymbol{v}} = 0. \tag{A.1}$$

Scaled successive differences,hence, will not yield a good estimation of $\dot{\boldsymbol{v}}$. In this section, an approach combining vector algebra and geometry is proposed.

We know from (A.1) that $\dot{\boldsymbol{v}}$ lies in a plane which has $\boldsymbol{v}$ as the normal vector. If the sampling rate is high enough, then the trajectory of $\boldsymbol{v}$ can be approximated as the arc$(\boldsymbol{\delta v})$ joining $\boldsymbol{v}_{\text{prev}}$ and $\boldsymbol{v}$. In Figure A.1, arc$(\boldsymbol{\delta v})$ is shown by the arc(AB) and the deviation from the assumption is denoted by arc(ACB). Using Gram-Schmidt Orthogonalization, we can say that

$$\dot{\boldsymbol{v}} \parallel (-(\boldsymbol{v}_{\text{prev}} - (\boldsymbol{v}.\boldsymbol{v}_{\text{prev}})\boldsymbol{v})). \tag{A.2}$$

The magnitude of $\dot{\boldsymbol{v}}$ cannot be approximated as $|(\boldsymbol{v} - \boldsymbol{v}_{\text{prev}})|$ for reasons mentioned earlier and can be determined as follows

$$|\dot{\boldsymbol{v}}| = \frac{\text{arc}(\boldsymbol{\delta v})}{h} = \frac{\theta}{h} \tag{A.3}$$

where θ is the angle between $\boldsymbol{v}$ and $\boldsymbol{v}_{\text{prev}}$ and h is the sampling time period. The constraint that $\boldsymbol{v} \in S^2$ is exploited to improve the accuracy of $|\dot{\boldsymbol{v}}|$ estimate.

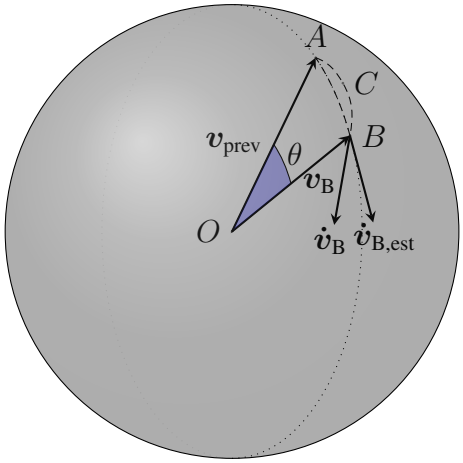

Figure A.1: Figure depicting the proposed estimator for $\dot{\boldsymbol{v}}$ for $\boldsymbol{v} \in S^2$ and the exaggerated error

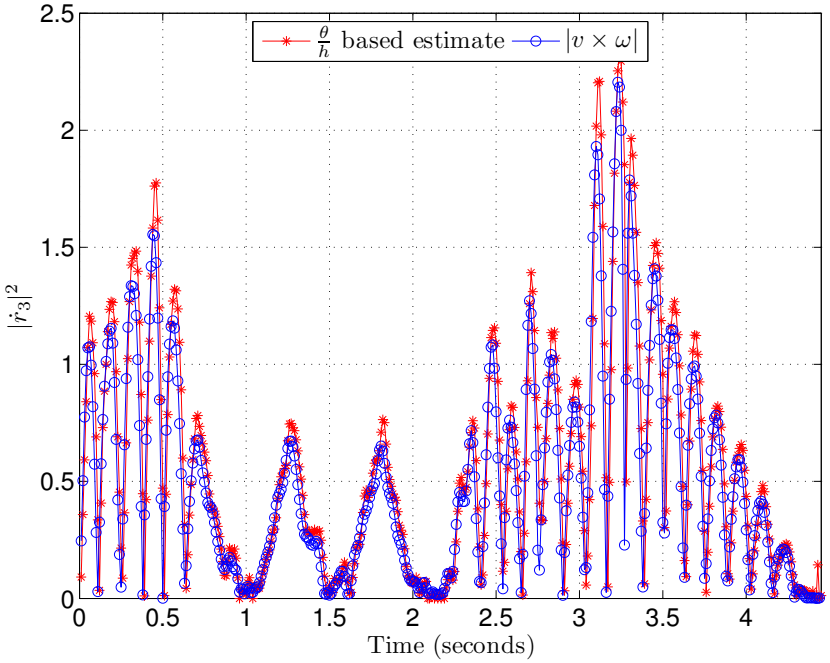

Figure A.2: Comparison of $|\dot{\boldsymbol{r}}_3|$ estimation using (3.16) and the discussion in Appendix A in Twin Rotor MIMO System discussed in Section 5.1

The relation (3.16) is compared with the derivative of the unit vector parallel to accelerometer using the estimator proposed in Appendix A. It should be noted that the estimate for $\frac{\theta}{h}$ was obtained completely from accelerometer whereas the estimate $|\boldsymbol{v} \times \boldsymbol{\omega}|$ has a rate gyro component involved. Figure A.2 displays a correlation of 92.52% substantiating the validity of the approximate estimate of $\dot{\boldsymbol{v}}$ discussed in Appendix A. Since roll-dynamics is absent, the deviations of the trajectory of the accelerometer from the coordinate plane is minimal, thereby strengthening the approximation.

The approximate method proposed in this section is a modification to the numerical

differentiation to compute the first derivative of a vector $\boldsymbol{v} \in S^2$. Based on the definition of $\boldsymbol{R}$ given in (2.1), we can use this method of estimating $\dot{\boldsymbol{v}}$ to estimate $\dot{\boldsymbol{R}}$ apart from the theoretical estimate given by $\dot{\boldsymbol{R}} = \boldsymbol{R}\hat{\boldsymbol{\omega}}$.

REFERENCES

[1] M. W. Spong, S. Hutchinson, and M. Vidyasagar, *Robot Modeling and Control*, 3rd ed. New York:Wiley, 2006.

[2] J. J. Craig, *Introduction to Robotics: Mechanics and Control*, 3rd ed. Englewood Cliffs, NJ:Prentice-Hall, 2003.

[3] L. Sciavicco and B. Siciliano, *Modeling and Control of Robot Manipulators*, 2nd ed. New York:Springer-Verlag, 2000.

[4] R. N. Murray, Z. Li, and S. Sastry, *A Mathematical Introduction to Robotics Manipulation*. CRC Press, 1994.

[5] T. Lee, M. Leok, and N. H. McClamroch, "Geometric tracking control of a Quadrotor UAV on SE(3)," *49th IEEE Conference on Decision and Control (CDC), Atlanta, GA*, pp. 5420–5425, 2010.

[6] J. R. Wertz, *Spacecraft Attitude Determination and Control*. Kluwer Academic Publishers, Dordrecht, 1978.

[7] M. D. Shuster and S. D. Oh, "Three-axis attitude determination from vector observations," *Journal of Guidance and Control*, vol. 4, no. 1, pp. 70–77, January-February 1981.

[8] G. Wahba, "A least squares estimate of satellite attitude," *SIAM Review*, vol. 7, no. 3, p. 409, 1965.

[9] M. Shuster, "Survey of attitude representations," *The Journal of the Astronautical Sciences*, vol. 41, no. 4, pp. 439–517, January-February 1981.

[10] R. Mahoney, T. Hamel, and J.-M. Pflimlin, "Nonlinear complementary filters on the special orthogonal group," *IEEE Transactions on Automatic Control*, vol. 53, no. 5, pp. 1203–1218, June 2008.

[11] N. Madinehi, "Rigid body attitude estimation: An overview and comparative study," *M.Sc Thesis, University of Western Ontario, Canada*, 2013.

[12] J. L. Crassidis, F. L. Markley, and Y. Cheng, "Survey of nonlinear attitude estimation methods," *Journal of Guidance and Control*, vol. 30, no. 1, pp. 12–28, January 2007.

[13] M. D. Shuster, "In quest of better attitudes," *Advances in the Astronautical Sciences*, vol. 108, pp. 2089–2117, 2001.

[14] S. Shen, Y. Mulgaonkar, N. Michael, and V. Kumar, "Vision-based state estimation for autonomous rotorcraft MAVs in complex environments," *International Conference on Robotics and Automation, Karlsruhe, Germany*, May 2013.

[15] Black, “A passive system for determining the attitude of a satellite,” *American Institute of Aeronautics and Astronautics (AIAA) Journal*, vol. 2, no. 7, pp. 1350–1351, 1964.

[16] W. Premerlani and P. Bizard, “Direction cosine matrix IMU: Theory,” May, 2009. [Online]. Available: gentlenav.googlecode.com/files/DCMDraft2.pdf

[17] V. Muralidharan and A. D. Mahindrakar, “Position stabilization and waypoint tracking control of mobile inverted pendulum robot,” *IEEE Transactions on Control Systems Technology*, vol. PP, p. 1, 2014.

[18] N. A. Chaturvedi, A. K. Sanyal, and N. H. McClamroch, “Rigid-body attitude control,” *IEEE Control Systems Magazine*, pp. 30–51, June 2011.

[19] O. Rodrigues, “Des lois géométriques qui régissent les déplacements d’un systéme solide dans l’espace, et de la variation des coordonnées provenant de ces déplacements considérés indépendamment des causes qui peuvent les produire,” *Journal de Mathématiques*, vol. 5, pp. 380–440, 1840.

[20] G. Piovan and F. Bullo, “On coordinate-free rotation decomposition: Euler angles about arbitrary axes,” *IEEE Transactions on Robotics*, vol. 28, no. 3, pp. 728–733, 2012.

[21] Press *et al.*, *Numerical Recipes - The Art of Scientific Computing (Third Edition)*. Cambridge Press, 2007.

[22] M. Grewal and A. Andrews, “How good is your gyro?” *IEEE Control Systems Magazine*, vol. 30, no. 1, pp. 12–86, 2010.

[23] “Sparkfun 9 degree-of-freedom Razor IMU,” 2014 April. [Online]. Available: https://www.sparkfun.com/products/10736